Non-oscillatory forward-in-time finite-volume methods for NWP

Christian Kühnlein

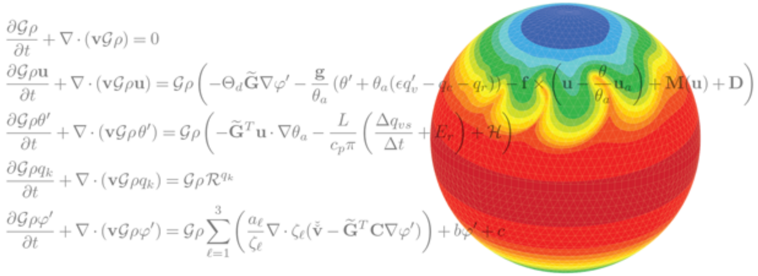

The atmospheric dynamical core plays a central role throughout IFS configurations

Forecast component	Description	#	Atmos. horiz. and vert. res.	Forecast length	3D ocean and sea-ice
4DVAR	Atm/land/waves High-resolution analysis	1	9 km 137 levels	-	-
EDA^{25}	Atm/land/waves Ensemble of data assimilations	25	18 km 137 levels	-	-
OCEAN5^{5} / ORAS5^{5}	3D ocean and sea-ice Ensemble of analyses	5	-	-	25 km 75 levels
HRES	Atm/land/waves/3D ocean High-resolution	1	9 km 137 levels	0-10 d	25 km 75 levels
ENS^{51}	Atm/land/wave/3D ocean Medium-range/monthly ensemble	51	9km L137 9km L137	0-15 d 15-46 d	25 km 75 levels
SEAS5^{51}	Atm/land/waves/3D ocean Seasonal ensemble	101	36 km 91 levels	0-7 m (0-13 m quarter)	25 km 75 levels

From June 2019, EDA with 50 members

for up-to-date information: https://confluence.ecmwf.int/display/FCST/Implementation+of+IFS+Cycle+49r1
(CY49r1 to be implemented 12 Nov 2024!)

Ocean – Land – Atmosphere – Sea ice

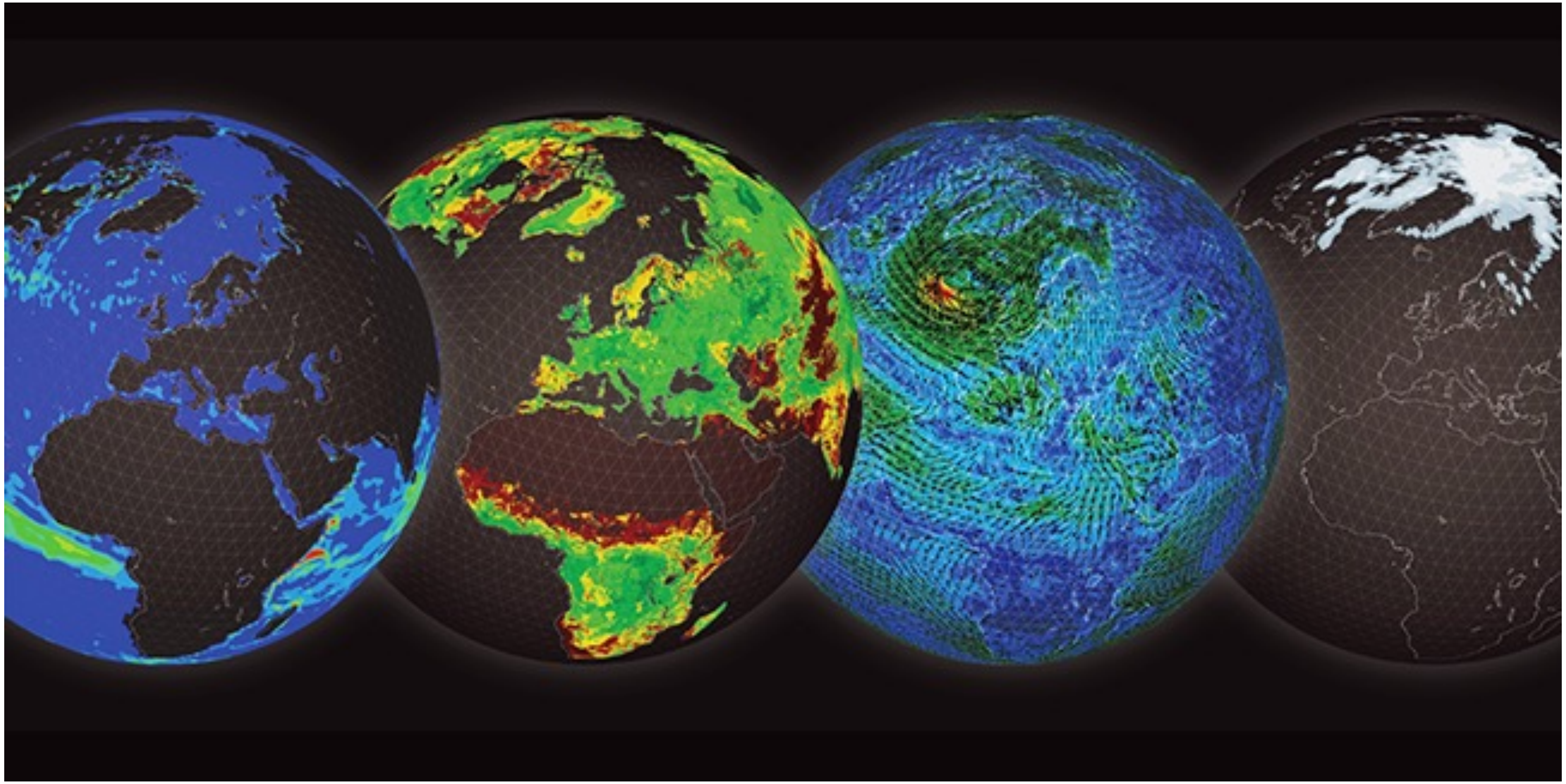

Spectral-transform formulation of the operational IFS (IFS-ST)

- hydrostatic primitive equations in hybrid mass-based vertical coordinate
- spherical-harmonics representation in horizontal
- finite-element approach for integrals in vertical
- two-time-level semi-implicit semi-Lagrangian integration scheme
- cubic-octahedral grid (“TCo“)
- coupling to IFS physics using SLAVEPP (Semi-Lagrangian Averaging of Physical Parametrisations)

Nodes of octadedral reduced Gaussian grid

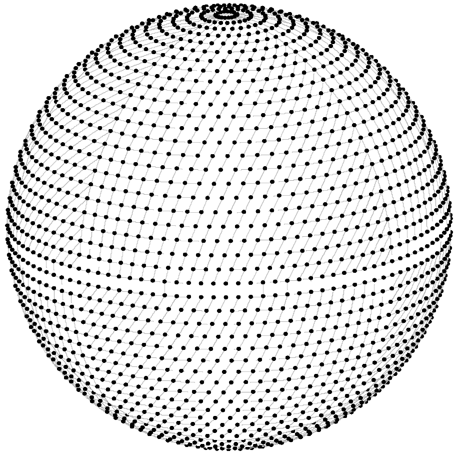

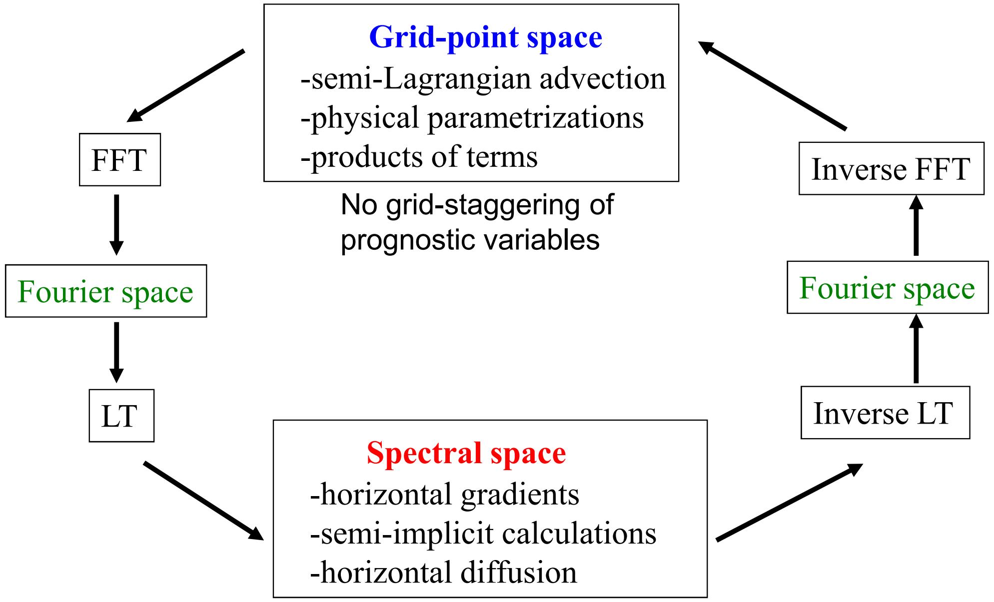

$$\psi(\lambda,\varphi) = \sum_{l=0}^{NSMAX} \sum_{-l\leq m\leq l} \psi_{l,m} Y_{l,m}(\lambda,\varphi)$$

IFS dynamical core performance comparison: time-to-solution at 3km for dry baroclinic instability test case with 10 tracer fields

Operational need!

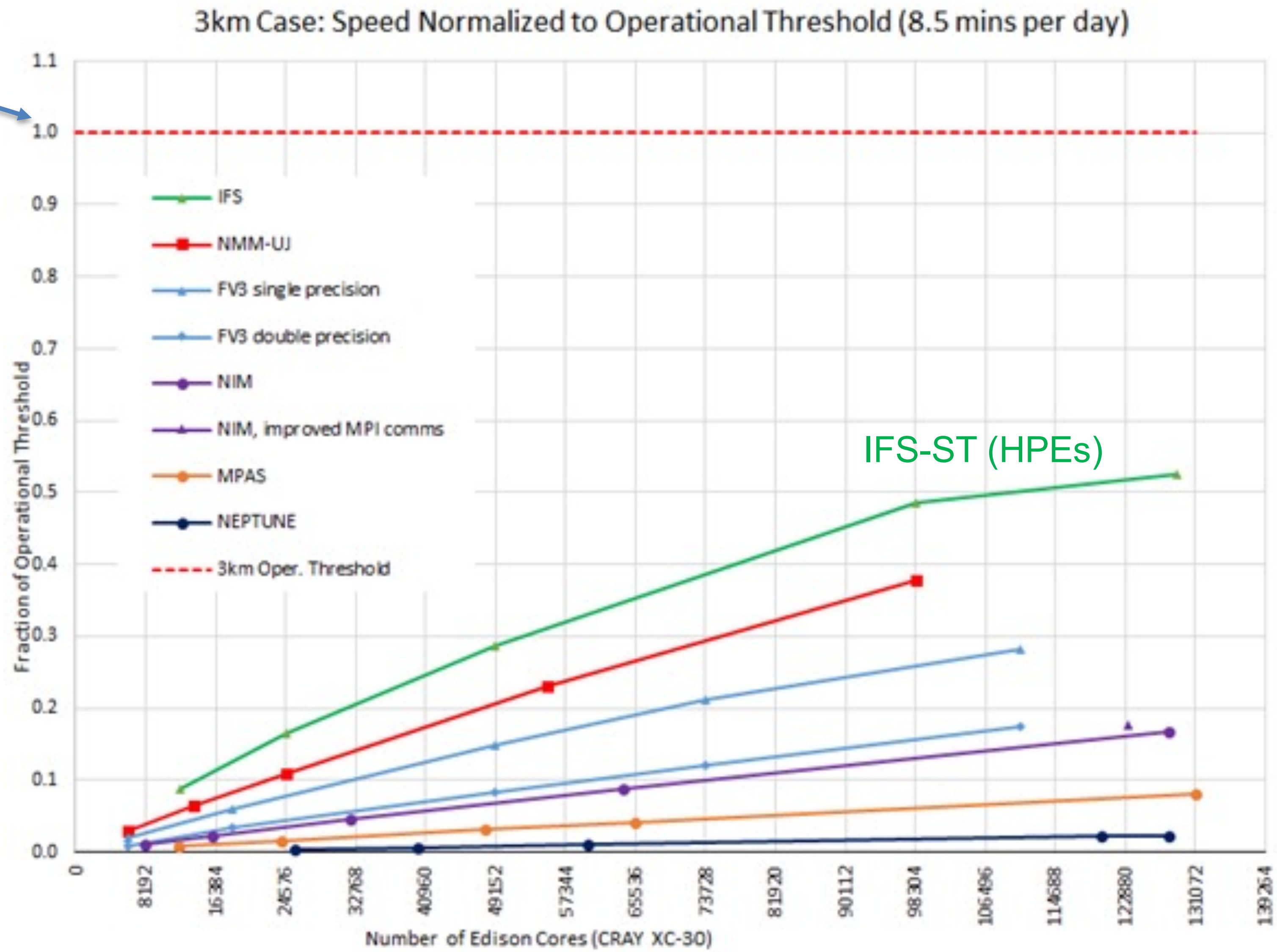

The higher the better

(adapted from Michalakes et al, NGGPS AVEC report, 2015)

IFS dynamical core performance comparison: time-to-solution at 3km for dry baroclinic instability test case with 10 tracer fields

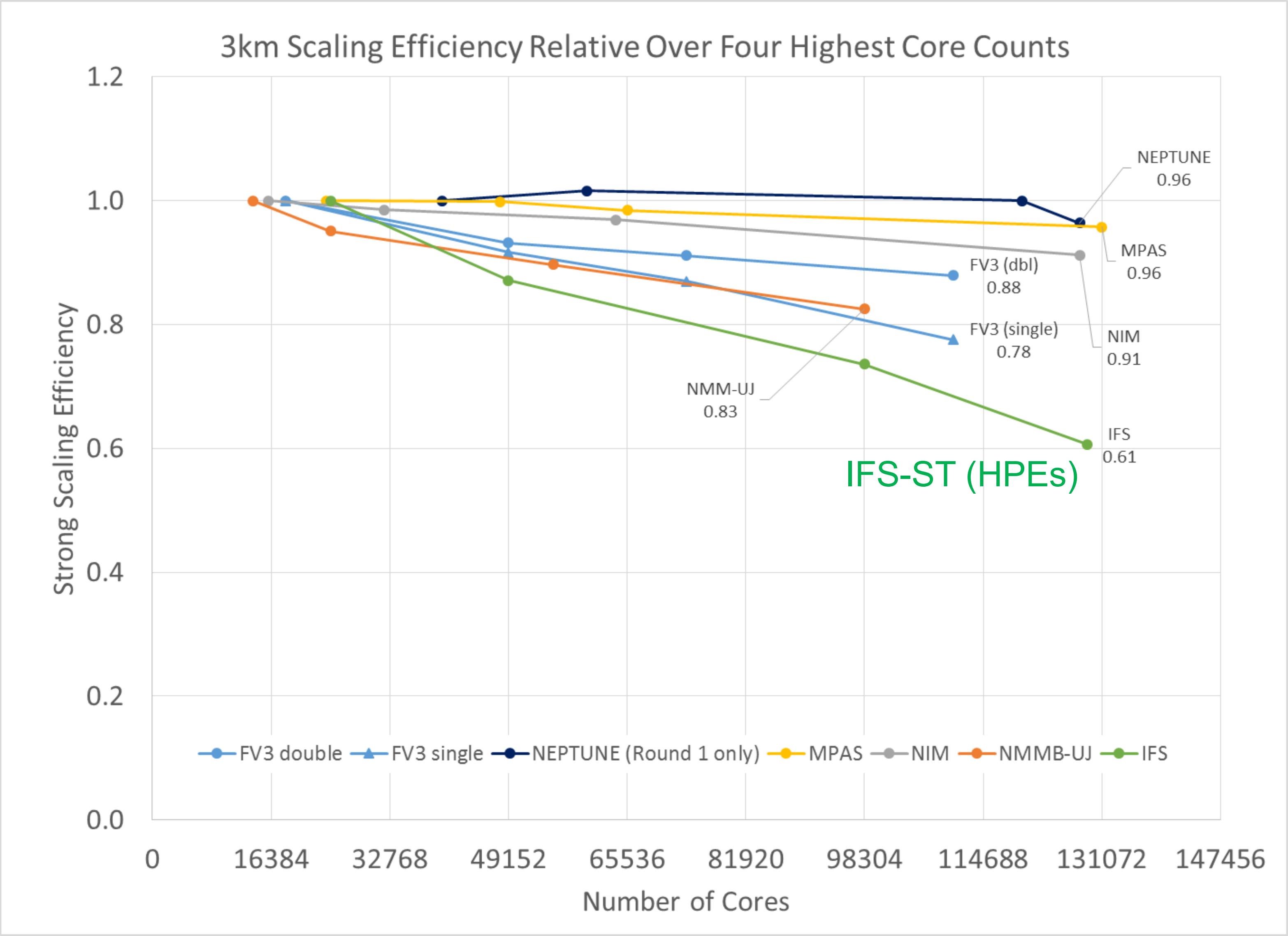

The higher the better

ECMWF EUROPEAN CENTRE FOR MEDIUM-RANGE WEATHER FORECASTS

(adapted from Michalakes et al, NGGPS AVEC report, 2015)

Current dynamical core options at ECMWF

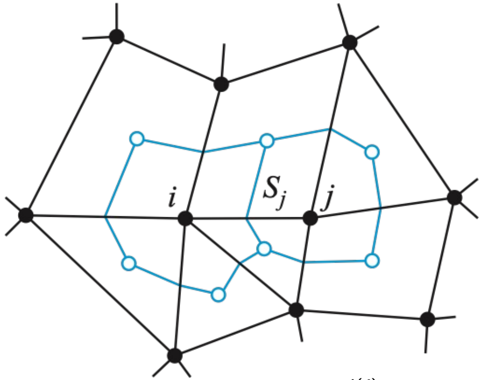

$$\int_\Omega \nabla\cdot\mathbf{A} = \int_{\partial\Omega}\mathbf{A}\cdot\mathbf{n} = \frac{1}{\mathcal{V}_i}\sum_{j=1}^{l(i)} A_j^{\perp} S_j$$

dual volume: $\mathcal{V}_i$, face area: S_j

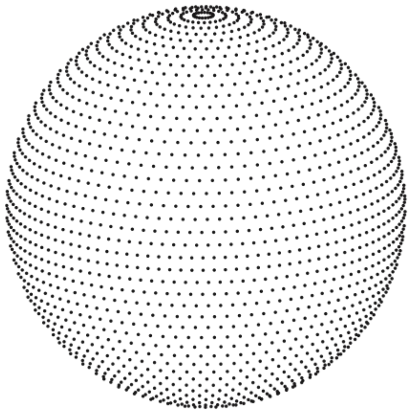

O24 grid points

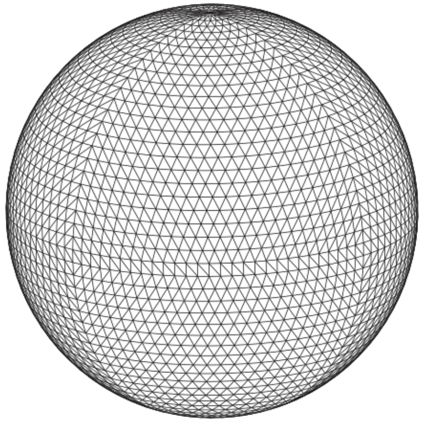

Primary mesh O24

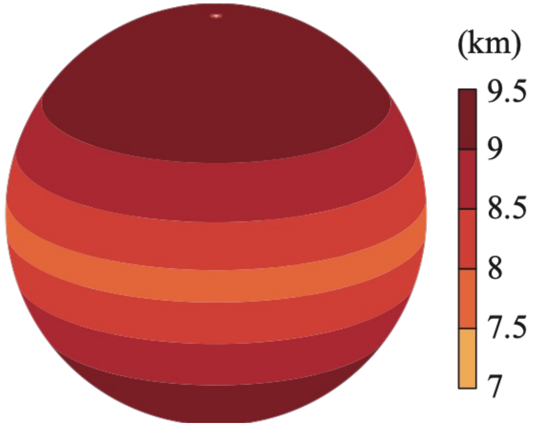

O1280 dual mesh spacing

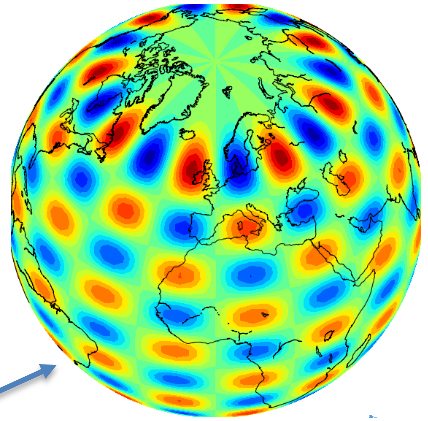

| currently operational |

Model aspect	IFS-FVM	IFS-ST	IFS-ST (NH option)
Equation system	fully compressible	hydrostatic primitive	fully compressible
Prognostic variables	$\rho_d, u, v, w, \theta', \varphi', r_v, r_l, r_r, r_i, r_s$	$\ln p_s, u, v, T_v, q_v, q_l, q_r, q_i, q_s$	$\ln \pi_s, u, v, d_4, T_v, \hat{q}, q_v, q_l, q_r, q_i, q_s$
Horizontal coordinates	λ, ϕ (lon–lat)	λ, ϕ (lon–lat)	λ, ϕ (lon–lat)
Vertical coordinate	generalized height	hybrid sigma–pressure	hybrid sigma–pressure
Horizontal discretization	unstructured finite volume (FV)	spectral transform (ST)	spectral transform (ST)
Vertical discretization	structured FD–FV	structured FE	structured FD or FE
Horizontal staggering	co-located	co-located	co-located
Vertical staggering	co-located	co-located	co-located, Lorenz
Horizontal grid	octahedral Gaussian or arbitrary	octahedral Gaussian	octahedral Gaussian
Time stepping scheme	2-TL SI	2-TL constant-coefficient SI	2-TL constant-coefficient SI with ICI
Advection	conservative FV Eulerian	non-conservative SL	non-conservative SL

FVM summary (from year 2019)

Current features:

- nonhydrostatic, deep-atmosphere, fully compressible equations
- horizontally-unstructured vertically-structured finite-volume discretisation
- semi-implicit integration with 3D implicit dynamics right-hand-sides (diffusion is HEVI by default)
- (explicit) nonoscillatory forward-in-time conservative Eulerian advection
- flexibility with respect to horizontal and vertical meshes
- Atlas library mesh and parallel datastructures
- Fortran code and using hybrid MPI/OpenMP for CPUs, but Python/GT4Py DSL implementation under development
- 64-bit or 32-bit precision
- IFS-FVM coupled to IFS physical parametrisation package (CY43R3)
- ecRad radiation scheme on model grid

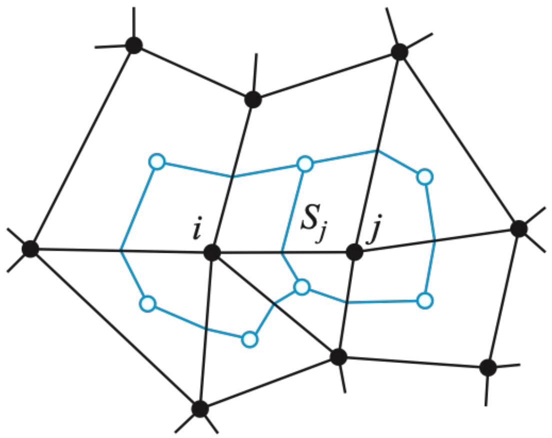

$$\int_\Omega \nabla\cdot\mathbf{A} = \int_{\partial\Omega} \mathbf{A}\cdot\mathbf{n} = \frac{1}{\mathcal{V}_i}\sum_{j=1}^{l(i)} A_j^{\perp} S_j$$

dual volume: $\mathcal{V}_i$, face area: S_j

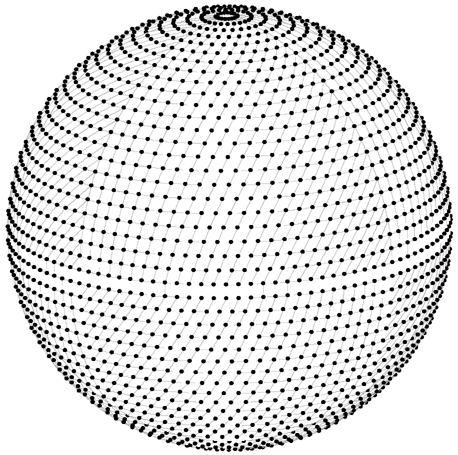

Nodes of octahedral grid O24

Octahedral reduced Gaussian grid of the IFS

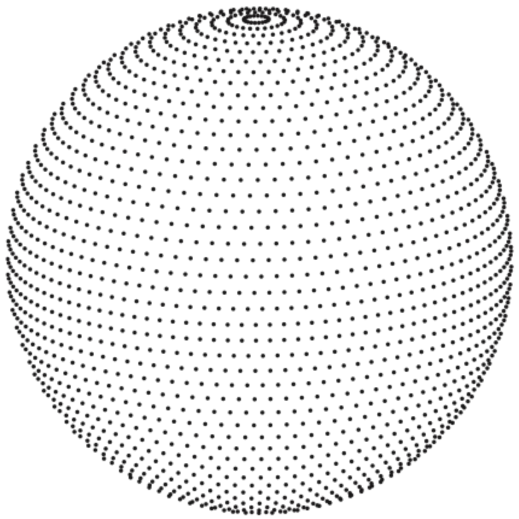

nodes of O24

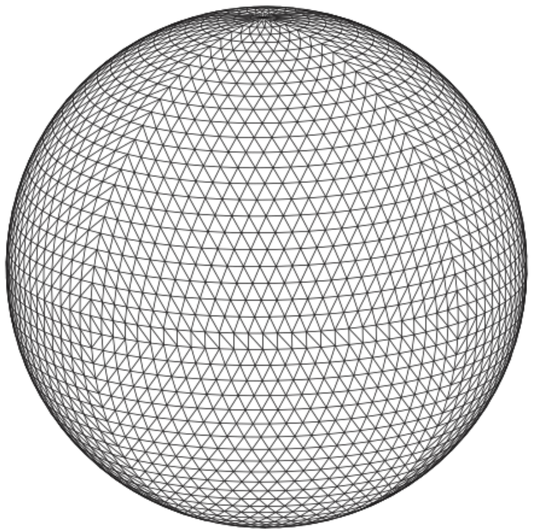

edges primary mesh connecting nodes of O24

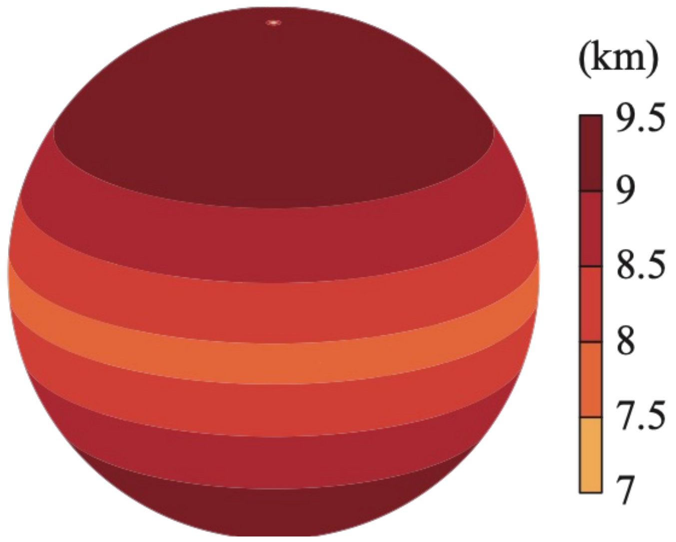

O1280 dual mesh spacing

- Quasi-uniform resolution over the surface of the sphere
- Suitable for spherical harmonics transforms and hence the spectral-transform IFS model
- Unstructured finite-volume IFS-FVM can develop mesh about nodes of the grid
- Using the same grid benefits overall infrastructure and model comparison studies

→ see Malardel et al. 2015; Smolarkiewicz et al. 2016; Deconinck et al. 2017; Kühnlein et al. 2019

Summary of FVM spatial discretization

- horizontally-unstructured finite-volume (FV) and vertically-structured finite-difference/finite-volume (FD/FV) discretisation framework
- median-dual FV approach is current default but other options are explored

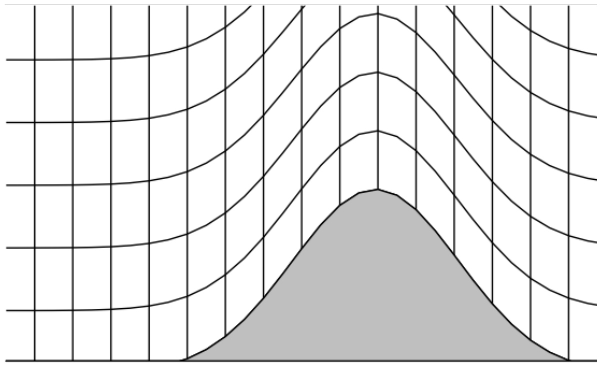

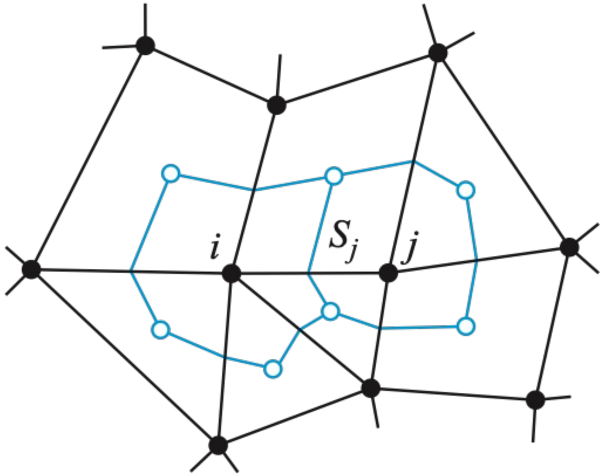

$$\int_{\Omega} \nabla \cdot \mathbf{A} = \int_{\partial\Omega} \mathbf{A} \cdot \mathbf{n} = \frac{1}{\mathcal{V}_i} \sum_{j=1}^{l(i)} A_j^{\perp} S_j$$

dual volume: $\mathcal{V}_i$, face area: S_j

- Gauss divergence theorem is central to FV technique
- Various approximations for FV fluxes between neighbouring cells depending on process and form of operator
- Fluxes in Laplacian operator (gradient & divergence) are usually linear & centred reconstructions of data at neighbouring points, compact specifications are used for diffusion, upwind and nonlinear fluxes occur in context of non-oscillatory advection

Smolarkiewicz et al. JCP 2016
Kühnlein et al. GMD 2019

FVM fully compressible equations with full IFS physics

$$\frac{\partial \mathcal{G}\rho_d}{\partial t} + \nabla \cdot (\mathbf{v}\mathcal{G}\rho_d) = 0\,,$$

$$\frac{\partial \mathcal{G}\rho_d \mathbf{u}}{\partial t} + \nabla \cdot (\mathbf{v}\mathcal{G}\rho_d \mathbf{u}) = \mathcal{G}\rho_d \left[-\theta_\rho \widetilde{\mathbf{G}} \nabla \varphi' - \theta_\rho \widetilde{\mathbf{G}} \nabla \varphi_a + \mathbf{g} - \mathbf{f} \times \mathbf{u} + \mathcal{M}(\mathbf{u}) + \boldsymbol{P}^{\mathbf{u}} \right]$$

$$\frac{\partial \mathcal{G}\rho_d \theta'}{\partial t} + \nabla \cdot \left(\mathbf{v}\mathcal{G}\rho_d\, \theta' \right) = \mathcal{G}\rho_d \left[-\mathbf{G}^T \mathbf{u} \cdot \nabla \theta_a + P^\theta \right]\,,$$

$$\frac{\partial \mathcal{G}\rho_d\, r_k}{\partial t} + \nabla \cdot (\mathbf{v}\mathcal{G}\rho_d\, r_k) = \mathcal{G}\rho_d P^{r_k}\,, \qquad r_k = r_v\,, r_l\,, r_r\,, r_i\,, r_s\,, \Lambda_a$$

$$\varphi = c_{pd} \left[\left(\frac{R_d}{p_0} \rho_d\, \theta\, (1 + r_v/\varepsilon) \right)^{R_d/c_{vd}} \right] = c_{pd}\pi$$

$$\theta_\rho = \frac{1 + r_v/\varepsilon}{1 + r_t} \theta$$

$$r_t = r_v + r_l + r_r + r_s + r_i$$

$$\varphi' = \varphi - \varphi_a\,, \qquad \theta' = \theta - \theta_a \qquad \mathbf{v} = \mathbf{G}^T \mathbf{u}$$

$$\epsilon = \frac{R_d}{R_v}$$

Universal characteristics of atmospheric flows

Universal characteristics of atmospheric motions (R. Klein *Annu. Rev. Fluid Mech. 2010)*

Earth's radius	$a \sim 6 \times 10^6$ m
Earth's rotation rate	$\Omega \sim 10^{-4}$ s^{-1}
Acceleration of gravity	$g \sim 9.81$ ms^{-2}
Sea-level pressure	$p_{\mathrm{ref}} \sim 10^5$ kgm^{-1} s^{-2}
H_2O freezing temperature	$T_{\mathrm{ref}} \sim 273$ K
Equator-pole potential temperature difference Tropospheric vertical potential temperature difference	$\Delta\Theta \sim 40$ K
Dry gas constant	$R = 287$ m^2 s^{-2} K^{-1}
Dry isentropic exponent	$\gamma = 1.4$

Auxiliary quantities of interest dervied from the Table above

Sea-level air density	$\rho_{\mathrm{ref}} = p_{\mathrm{ref}}/(RT_{\mathrm{ref}}) \sim 1.25$ kgm^{-3}
Density scale height	$h_{\mathrm{sc}} = \gamma p_{\mathrm{ref}}/(g\rho_{\mathrm{ref}}) \sim 11$ km
Sound speed	$c_{\mathrm{ref}} = \sqrt{\gamma p_{\mathrm{ref}}/\rho_{\mathrm{ref}}} \sim 330$ ms^{-1}
Internal wave speed	$c_{\mathrm{int}} = \sqrt{g h_{\mathrm{sc}} \frac{\Delta\Theta}{T_{\mathrm{ref}}}} \sim 110$ ms^{-1}
Thermal wind velocity	$u_{\mathrm{ref}} = \frac{2}{\pi} \frac{g h_{\mathrm{sc}}}{\Omega a} \frac{\Delta\Theta}{T_{\mathrm{ref}}} \sim 12$ ms^{-1}

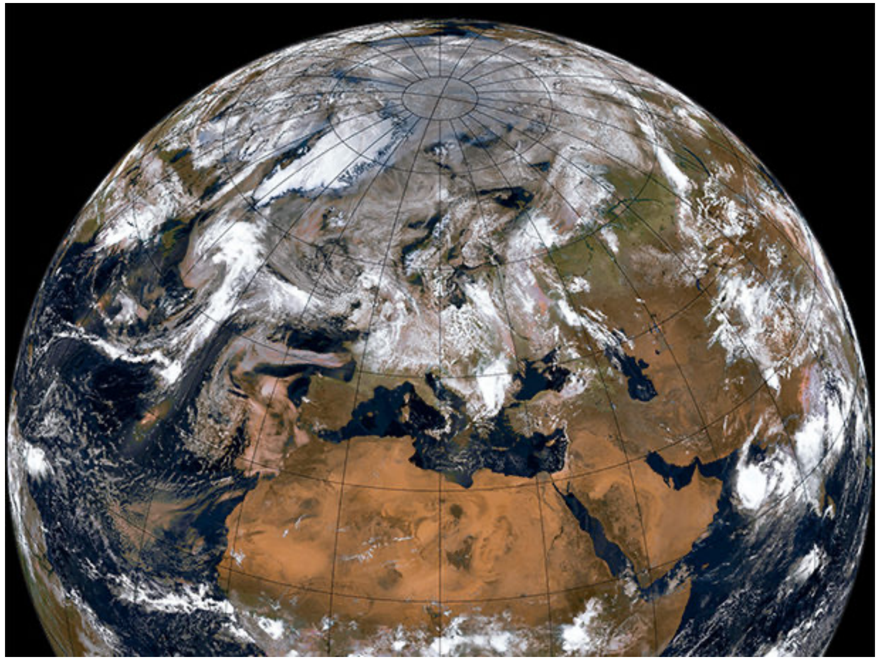

Courtesy EUMETSAT

FVM semi-implicit integration

$$\frac{\partial G\Psi}{\partial t} + \nabla \cdot (\boldsymbol{V}\Psi) = G\left(\mathcal{R}^\Psi + P^\Psi\right) ,$$

$$\Psi_{\boldsymbol{i}}^{n+1} = \mathcal{A}_{\boldsymbol{i}}(\widetilde{\Psi}, \boldsymbol{V}^{n+1/2}, G^n, G^{n+1}, \delta t) + b^\Psi \, \delta t \, \mathcal{R}^\Psi|_{\boldsymbol{i}}^{n+1}$$
$$\equiv \widehat{\Psi}_{\boldsymbol{i}} + b^\Psi \, \delta t \, \mathcal{R}^\Psi|_{\boldsymbol{i}}^{n+1} ,$$

$$\widetilde{\Psi} = \Psi^n + a^\Psi \, \delta t \, \mathcal{R}^\Psi|^n + \delta t \, P^\Psi|^n ,$$

Variable	Ψ	$\boldsymbol{V}$	G	a^Ψ	b^Ψ
Dry density	ρ_d	$\boldsymbol{v}\mathcal{G}$	$\mathcal{G}$	–	–
Zonal physical velocity	u	$\boldsymbol{v}\mathcal{G}\rho_d$	$\mathcal{G}\rho_d$	0.5	0.5
Meridional physical velocity	v	$\boldsymbol{v}\mathcal{G}\rho_d$	$\mathcal{G}\rho_d$	0.5	0.5
Vertical physical velocity	w	$\boldsymbol{v}\mathcal{G}\rho_d$	$\mathcal{G}\rho_d$	0.5	0.5
Potential temperature perturbation	θ'	$\boldsymbol{v}\mathcal{G}\rho_d$	$\mathcal{G}\rho_d$	0.5	0.5
Water vapour mixing ratio	r_v	$\boldsymbol{v}\mathcal{G}\rho_d$	$\mathcal{G}\rho_d$	–	–
Liquid water mixing ratio	r_l	$\boldsymbol{v}\mathcal{G}\rho_d$	$\mathcal{G}\rho_d$	–	–
Rain water mixing ratio	r_r	$\boldsymbol{v}\mathcal{G}\rho_d$	$\mathcal{G}\rho_d$	–	–
Ice mixing ratio	r_i	$\boldsymbol{v}\mathcal{G}\rho_d$	$\mathcal{G}\rho_d$	–	–
Snow mixing ratio	r_s	$\boldsymbol{v}\mathcal{G}\rho_d$	$\mathcal{G}\rho_d$	–	–
Cloud fraction	Λ_a	$\boldsymbol{v}\mathcal{G}\rho_d$	$\mathcal{G}\rho_d$	–	–
Exner pressure perturbation	φ'	$\boldsymbol{v}\mathcal{G}\rho_d$	$\mathcal{G}\rho_d$	$(1-\alpha)$	α

Main principles of default scheme:

- Time integration aims for a high degree of implicitness with respect to rhs forcings
- Focus on co-located arrangement of prognostic variables, but selected compact operators used
- Numerically consistent second-order design about non-oscillatory forward-in-time flux-form advection (core design uses MPDATA, alternative transport schemes for selected variables and tracers incorporated)
- Compact-stencil diffusion with implicit time stepping

FVM coupling to IFS physical parametrisations

Bauer et al. Nature 2015

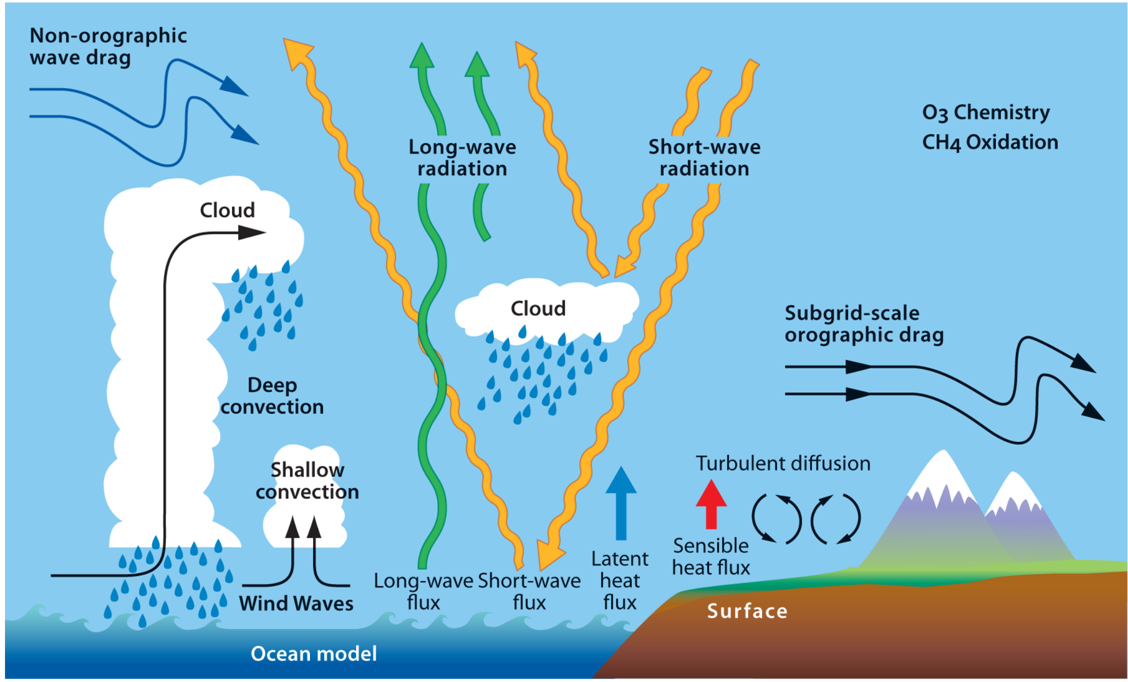

- Parametrizations for turbulence, convection, cloud microphysics, orographic and non-orographic gravity wave drag
- Land surface model HTESSEL
- ecRad radiation scheme on model grid (called every 1h)
- As the current default, tendencies from IFS physical parametrizations are incorporated in FVM SI scheme using Euler forward approach with subcycling of dynamics:

$$\text{Physics time step from } t^N \text{ to } t^N + \Delta t_{phys} \equiv t^N + N_s\,\delta t \text{ for } \ell = 1, N_s :$$

$$\Psi_{\mathbf{i}}\big(t^N + \ell\delta t\big) = \mathscr{A}_{\mathbf{i}}\big(\widetilde{\Psi}, \mathbf{V}(t^N + (\ell\delta t - 0.5)), G(t^N + (\ell-1)\delta t), G(t^N + \ell\delta t), \delta t\big) + b^{\Psi}\,\delta t\,\mathscr{R}_{\mathbf{i}}^{\Psi}\big(t^N + \ell\delta t\big)$$

$$\widetilde{\Psi} = \Psi\big(t^N + (\ell-1)\delta t\big) + a^{\Psi}\,\delta t\,\mathscr{R}^{\Psi}\big(t^N + (\ell-1)\delta t\big) + \delta t\, P^{\Psi}\big(t^N, \Delta t_{phys}\big)$$

Fundamentals of the FVM integration scheme

Lagrangian $\dfrac{d\psi}{dt} = R^{\psi}$

Eulerian $\dfrac{\partial G\Psi}{\partial t} + \nabla \cdot (\mathbf{V}\Psi) = G\,\mathcal{R}^{\Psi}$

Eulerian-Lagrangian congruency

$$\Psi_{\mathbf{i}}^{n+1} = \mathcal{A}_{\mathbf{i}}(\widetilde{\Psi}, \mathbf{V}^{n+1/2}, G^{n}, G^{n+1}, \delta t) + b^{\Psi}\,\delta t\,\mathcal{R}^{\Psi}\big|_{\mathbf{i}}^{n+1}$$

with $\widetilde{\Psi} = \Psi^{n} + a^{\Psi}\,\delta t\,\mathcal{R}^{\Psi}\big|^{n}$

Forward-in-time discretization: $\dfrac{G^{n+1}\Psi^{n+1} - G^{n}\Psi^{n}}{\delta t} + \nabla \cdot \left(\mathbf{V}^{n+1/2}\Psi^{n}\right) = \left(G\mathcal{R}^{\Psi}\right)^{n+1/2}$

Modified equation:

$$\frac{\partial G\Psi}{\partial t} + \nabla \cdot (\mathbf{V}\Psi) = G\mathcal{R}^{\Psi} - \nabla \cdot \left\{ \frac{\delta t}{2}\mathbf{V}\left[\frac{1}{G}\nabla \cdot (\mathbf{V}\Psi) + \frac{\Psi}{G}\frac{\partial G}{\partial t}\right]\right\} + \nabla \cdot \left(\mathbf{V}\mathcal{R}^{\Psi}\frac{\delta t}{2}\right) + \mathcal{O}(\delta t^{2})$$

→ See Piotr Smolarkiewicz's lecture for further discussion

MPDATA scheme

- MPDATA: Multidimensional Positive Definite Advection Transport Algorithm
- Upwind scheme followed by error-compensating steps formulated as pseudo-flux achieves at least second-order accurate solution
- Limiting the pseudo-flux using Flux-Corrected Transport approach achieves monotone solution
- Many variants of the scheme exist (sign-preserving, split vs unsplit, third-order extension, structured grids, unstructured meshes, curvilinear coordinates, moving meshes)

➢ Smolarkiewicz (1983); Smolarkiewicz and Clark (1986); Smolarkiewicz and Grabowski (1990); Smolarkiewicz and Margolin (1998); Smolarkiewicz and Szmelter (2005); Kühnlein et al. 2012; Kühnlein and Smolarkiewicz (2017); Waruszewski et al. 2018

$$
\begin{aligned}
\Psi_{\mathbf{i}}^{n+1} &= \mathcal{A}_{\mathbf{i}}(\Psi^n, \mathbf{V}^{n+1/2}, G^n, G^{n+1}) \\
&= \chi_{\mathbf{i}}^{n+1/2}\, \widetilde{\mathcal{A}}_{\mathbf{i}}(\Psi^n, \mathbf{V}^{n+1/2}, G^n, G^{n+1}) \\
&= \chi_{\mathbf{i}}^{n+1/2}\, \Psi_{\mathbf{i}}^{\mathcal{N}_\eta}
\end{aligned}
$$

where $\chi^{n+1/2} \equiv \dfrac{G^n}{G^{n+1}}$

$\widetilde{\mathcal{A}}_{\mathbf{i}}$ iterates for $\eta = 1, \mathcal{N}_\eta$:

$$
\begin{aligned}
\Psi_{k,i}^{(\eta)} = \Psi_{k,i}^{(\eta-1)} &- \frac{\delta t}{G_{k,i}^n\, \mathcal{V}_i} \sum_{j=1}^{l(i)} F_{k,j}^{\perp}\left(\Psi_{k,i}^{(\eta-1)}, \Psi_{k,j}^{(\eta-1)}, V_{k,j}^{\perp\,(\eta)}\right) S_j \\
&- \frac{\delta t}{G_{k,i}^n\, \delta z} \Bigg\{ F_{k+1/2,i}^{z}\left(\Psi_{k,i}^{(\eta-1)}, \Psi_{k+1,i}^{(\eta-1)}, V_{k+1/2,i}^{z\,(\eta)}\right) \\
&\qquad - F_{k-1/2,i}^{z}\left(\Psi_{k-1,i}^{(\eta-1)}, \Psi_{k,i}^{(\eta-1)}, V_{k-1/2,i}^{z\,(\eta)}\right)\Bigg\}
\end{aligned}
$$

Split Eulerian flux-form advection

Mass-compatible horizontal-vertical Strang-split flux-form advection in FVM:

$$\rho_{\mathrm{d}\,\boldsymbol{i}}^{[1]} = \mathcal{A}_{\boldsymbol{i}}^{z}(\rho_{\mathrm{d}}^{n}, (v^{z}\mathcal{G})^{n+1/2}, \mathcal{G}^{n}, \mathcal{G}^{[1]}, 0.5\delta t)\ ,$$
$$\rho_{\mathrm{d}\,\boldsymbol{i}}^{[2]} = \mathcal{A}_{\boldsymbol{i}}^{xy}(\rho_{\mathrm{d}}^{[1]}, (\boldsymbol{v}_{\mathrm{h}}\mathcal{G})^{n+1/2}, \mathcal{G}^{[1]}, \mathcal{G}^{[2]}, \delta t)\ ,$$
$$\rho_{\mathrm{d}\,\boldsymbol{i}}^{n+1} = \rho_{\mathrm{d}\,\boldsymbol{i}}^{[3]} = \mathcal{A}_{\boldsymbol{i}}^{z}(\rho_{\mathrm{d}}^{[2]}, (v^{z}\mathcal{G})^{n+1/2}, \mathcal{G}^{[2]}, \mathcal{G}^{n+1}, 0.5\delta t)$$

$$\Psi_{\boldsymbol{i}}^{[1]} = \mathcal{A}_{\boldsymbol{i}}^{z}(\widetilde{\Psi}, (v^{z}\mathcal{G}\rho_{\mathrm{d}})^{[1]}, (\mathcal{G}\rho_{\mathrm{d}})^{n}, (\mathcal{G}\rho_{\mathrm{d}})^{[1]}, 0.5\delta t)\ ,$$
$$\Psi_{\boldsymbol{i}}^{[2]} = \mathcal{A}_{\boldsymbol{i}}^{xy}(\Psi^{[1]}, (v_{\mathrm{h}}^{\perp}\mathcal{G}\rho_{\mathrm{d}})^{[2]}, (\mathcal{G}\rho_{\mathrm{d}})^{[1]}, (\mathcal{G}\rho_{\mathrm{d}})^{[2]}, \delta t)\ ,$$
$$\Psi_{\boldsymbol{i}}^{[3]} = \mathcal{A}_{\boldsymbol{i}}^{z}(\Psi^{[2]}, (v^{z}\mathcal{G}\rho_{\mathrm{d}})^{[3]}, (\mathcal{G}\rho_{\mathrm{d}})^{[2]}, (\mathcal{G}\rho_{\mathrm{d}})^{n+1}, 0.5\delta t)$$

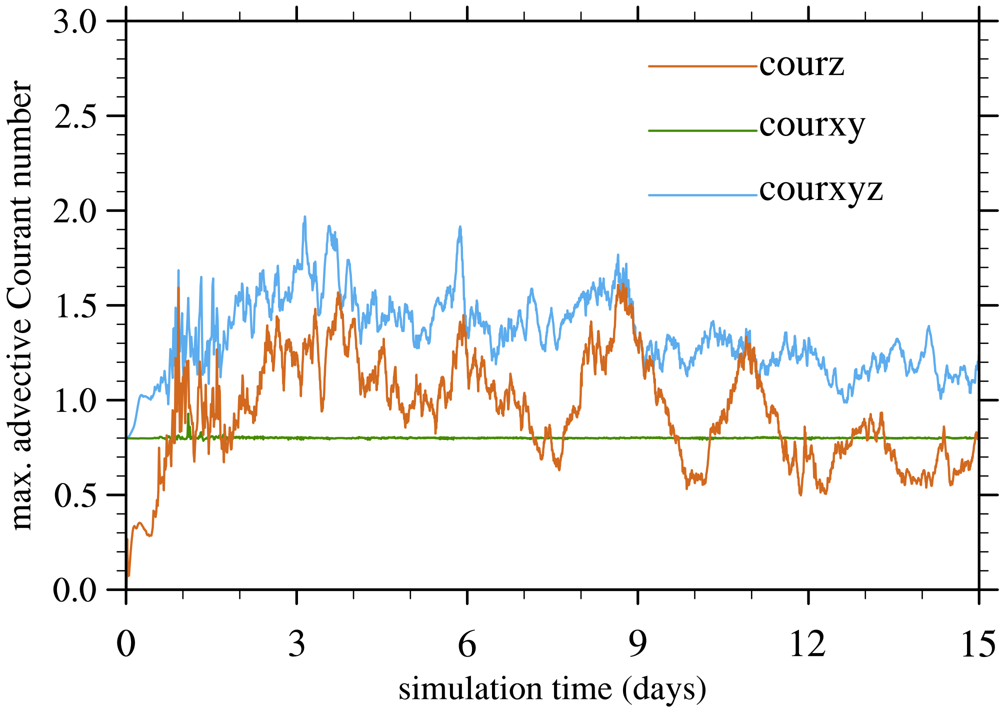

Kühnlein et al. GMD 2019

ECMWF

Formulate Schur complement

$$r_{l\,\mathbf{i}}^{\,n+1} = \widehat{r_l}_{\mathbf{i}}\,, \quad r_{r\,\mathbf{i}}^{\,n+1} = \widehat{r_r}_{\mathbf{i}}\,, \quad r_{i\,\mathbf{i}}^{\,n+1} = \widehat{r_i}_{\mathbf{i}}\,, \quad r_{s\,\mathbf{i}}^{\,n+1} = \widehat{r_s}_{\mathbf{i}}$$

$$r_{v\,\mathbf{i}} = \widehat{r_v}_{\mathbf{i}} + \delta t_h \left[-\alpha_{r_v}(r_v - r_{vr})\right]_{\mathbf{i}}$$

$$\theta_{\mathbf{i}} = \widehat{\theta}_{\mathbf{i}} + \delta t_h \left[-\alpha_\theta(\theta - \theta_r)\right]_{\mathbf{i}} \qquad \theta_\rho^\star = \theta^\star \vartheta^{n+1} \equiv \frac{\theta^\star(1 + r_v^{n+1}/\varepsilon)}{(1 + r_t^{n+1})}$$

$$\theta'_{\mathbf{i}} = \widehat{\theta'}_{\mathbf{i}} + \delta t_h \left[-\widetilde{\mathbf{G}}^T \mathbf{u} \cdot \nabla\theta_a - \alpha_\theta\theta' - \alpha_\theta(\theta_a - \theta_r)\right]_{\mathbf{i}}$$

$$\mathbf{u}_{\mathbf{i}} = \widehat{\mathbf{u}}_{\mathbf{i}} + \delta t_h \left[-\theta^\star\vartheta^{n+1}\widetilde{\mathbf{G}}\nabla\varphi' - (\theta_a + \theta')\,\vartheta^{n+1}\widetilde{\mathbf{G}}\nabla\varphi_a + \mathbf{g} - \mathbf{f}\times\mathbf{u} + \mathcal{M}^\star(\mathbf{u}^\star, \mathbf{u}) - \alpha_{\mathbf{u}}(\mathbf{u} - \mathbf{u}_r)\right]_{\mathbf{i}}$$

$$\mathbf{L}\,\mathbf{u} = \widehat{\widehat{\mathbf{u}}} - \delta t_h\, \theta_\rho^\star\, \widetilde{\mathbf{G}}\nabla\varphi' \longrightarrow \mathbf{u} = \mathbf{L}^{-1}\widehat{\widehat{\mathbf{u}}} - \mathbf{L}^{-1}\delta t_h\, \theta_\rho^\star\, \widetilde{\mathbf{G}}\nabla\varphi' \longrightarrow$$

$$\boxed{\begin{aligned} &\mathbf{u} = \bar{\mathbf{u}} - \mathbf{C}\nabla\varphi' \\ &\bar{\mathbf{u}} = \mathbf{L}^{-1}\widehat{\widehat{\mathbf{u}}} \qquad \mathbf{C} = \mathbf{L}^{-1}\delta t_h\, \theta_\rho^\star\, \widetilde{\mathbf{G}} \end{aligned}}$$

Helmholtz equation for implicit treatment of Exner pressure

Total derivative of equation of state combined with mass continuity, thermodynamic, and water vapour mixing ratio equations yields, see Smolarkiewicz et al. (2014, 2017, 2019); Kühnlein et al. 2019:

$$\frac{\partial(\mathcal{G}\rho_d\varphi')}{\partial t} + \nabla\cdot\left(\mathbf{v}\mathcal{G}\rho_d\varphi'\right) = \mathcal{G}\rho_d\left[-\frac{\xi\varphi}{\mathcal{G}}\nabla\cdot\left(\mathcal{G}\mathbf{G}^T\mathbf{u}\right) - \frac{1}{\mathcal{G}\rho_d}\nabla\cdot\left(\mathcal{G}\rho_d\varphi_a\mathbf{G}^T\mathbf{u}\right)\right.$$
$$\left. + \frac{\varphi_a}{\mathcal{G}\rho_d}\nabla\cdot\left(\mathcal{G}\rho_d\mathbf{G}^T\mathbf{u}\right) - \frac{\partial\varphi_a}{\partial t} + P^{\varphi}\right]$$

with $$P^{\varphi} = \xi\varphi\left(\frac{P^{\theta}}{\theta} + \frac{P^{r_v}/\varepsilon}{1 + r_v/\varepsilon}\right) \qquad \xi = \frac{R_d}{c_{vd}}$$

$$\varphi'_{\mathbf{i}} = \mathcal{A}(\varphi'^n + (1-\beta)\,\delta t\,\mathcal{R}^{\varphi'}|^n + \delta t\,P^{\varphi'}|^n, (\mathbf{v}\mathcal{G}\rho_d)^{\perp}|^{n+1/2}, (\mathcal{G}\rho_d)^n, (\mathcal{G}\rho_d)^{n+1}, \delta t) + \beta\,\delta t\,\mathcal{R}^{\varphi'}|^{n+1}$$

$$\beta \in [0.5, 1.0]$$

Elliptic Helmholtz boundary value problem

$$\boxed{0 = -\sum_{\ell=1}^{3}\left(\frac{A_\ell^\star}{\zeta_\ell}\nabla\cdot\zeta_\ell\,\widetilde{\mathbf{G}}^T(\overline{\mathbf{u}} - \mathbf{C}\nabla\varphi')\right) - B^\star(\varphi' - \widehat{\varphi'}) \quad\equiv\quad \mathcal{L}(\varphi') - R}$$

Coefficients:

$$A_1^\star = 1\,,\qquad A_2^\star = \frac{c_{vd}}{R_d}\frac{\varphi_a}{\varphi} = -A_3^\star\,,\qquad \zeta_1 = \mathcal{G}\,,\quad \zeta_2 = \mathcal{G}\rho_d\varphi_a\,,\quad \zeta_3 = \mathcal{G}\rho_d\,,\qquad B^\star = \frac{1}{\beta\,\delta t}\frac{c_{vd}}{R_d\,\varphi}$$

Advective part:

$$\widehat{\varphi'} = \mathcal{A}(\varphi'^n + (1-\beta)\,\delta t\,\mathcal{R}^{\varphi'}|^n + \delta t\,P^{\varphi'}|^n, (\mathbf{v}\mathcal{G}\rho_d)^\perp|^{n+1/2}, (\mathcal{G}\rho_d)^n, (\mathcal{G}\rho_d)^{n+1}, \delta t)$$

- 3D implicit Exner pressure solution is a crucial aspect for the performance, robustness and accuracy of the FVM model
- Different kinds of solution methods considered/developed as some future HPC architectures may require approaches that operate within the acoustic radius

Linear solvers for the 3D Helmholtz problem

- We prefer the Generalized Conjugate Residual method of order *k* for non-symmetric systems (GMRES, BiCGSTAB are alternatives, pipelined versions can be useful)
- Matrix-free implementation
- Bespoke preconditioners for atmospheric configurations
- Multi-grid extension for preconditioner (Gillard et al. 2024)

➢ See Smolarkiewicz et al. (2000, 2004); Smolarkiewicz and Szmelter 2011 for tutorials

Weighted line Jacobi method preconditioner in FVM (Kühnlein et al. 2019):

$$e^{\mu+1} = \omega\left[\mathcal{D}+\mathcal{P}_z\right]^{-1}\left(\mathcal{D}e^{\mu}-\mathcal{P}_\mathrm{h}(e^{\mu})+\hat{r}\right)+(1-\omega)\,e^{\mu}$$

$$\mathcal{D}_{k,i} = -\frac{1}{4\mathcal{V}_\mathrm{i}}\sum_{\ell=1}^{3}\frac{A^{\star}_{\ell k,i}}{\zeta_{\ell k,i}}\sum_{j=1}^{l(i)}\frac{\zeta_{\ell k,j}}{\mathcal{V}_j}\left(\mathcal{B}^{11}_{k,j}S_j^{x\,2}+\mathcal{B}^{22}_{k,j}S_j^{y\,2}\right)$$

For $n = 1,2,\ldots$ until convergence do

for $\nu = 0,\ldots,k-1$ do

$$\beta = -\frac{\langle r^{\nu}\,\mathcal{L}(q^{\nu})\rangle}{\langle \mathcal{L}(q^{\nu})\mathcal{L}(q^{\nu})\rangle}\,,$$

$$\psi_\mathrm{i}^{\nu+1} = \psi_\mathrm{i}^{\nu} + \beta q_\mathrm{i}^{\nu}\,,$$

$$r_\mathrm{i}^{\nu+1} = r_\mathrm{i}^{\nu} + \beta\mathcal{L}_\mathrm{i}(q^{\nu})\,,$$

$$\text{exit if } \|r^{\nu+1}\| \le \epsilon\,,$$

$$e_\mathrm{i} = \mathcal{P}_\mathrm{i}^{-1}(r^{\nu+1})\,,$$

$$\text{evaluate } \mathcal{L}_\mathrm{i}(e)\,,$$

$$\forall_{l=0,\nu}\ \alpha_l = -\frac{\langle \mathcal{L}(e)\mathcal{L}(q^l)\rangle}{\langle \mathcal{L}(q^l)\mathcal{L}(q^l)\rangle}\,,$$

$$q_\mathrm{i}^{\nu+1} = e_\mathrm{i} + \sum_{l=0}^{\nu}\alpha_l q_\mathrm{i}^l\,,$$

$$\mathcal{L}_\mathrm{i}(q^{\nu+1}) = \mathcal{L}_\mathrm{i}(e) + \sum_{l=0}^{\nu}\alpha_l\,\mathcal{L}_\mathrm{i}(q^l)\,,$$

end do ,

reset $(\psi, r, q, \mathcal{L}(q))_\mathrm{i}^k$ to $[\psi, r, q, \mathcal{L}(q)]_\mathrm{i}^0$,

end do .

GCR(k) scheme

FVM comparison to hydrostatic IFS-ST: dry adiabatic dynamics

surface pressure (hPa) at day 10

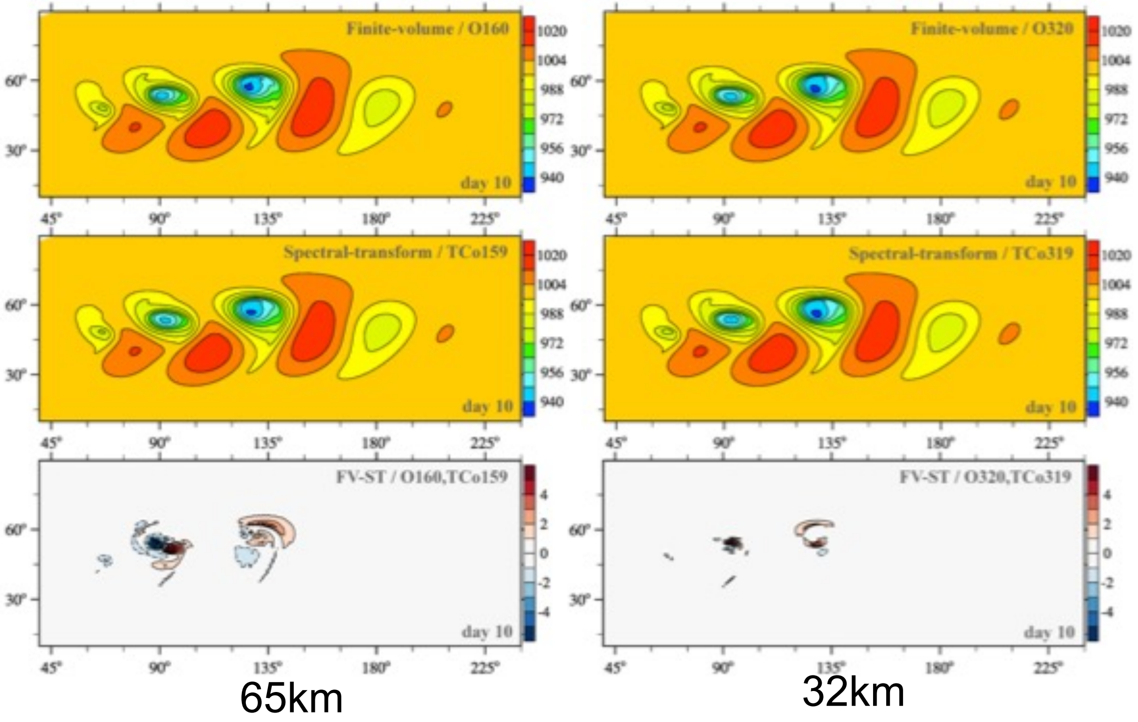

meridional wind (m/s) at 50N at day 10

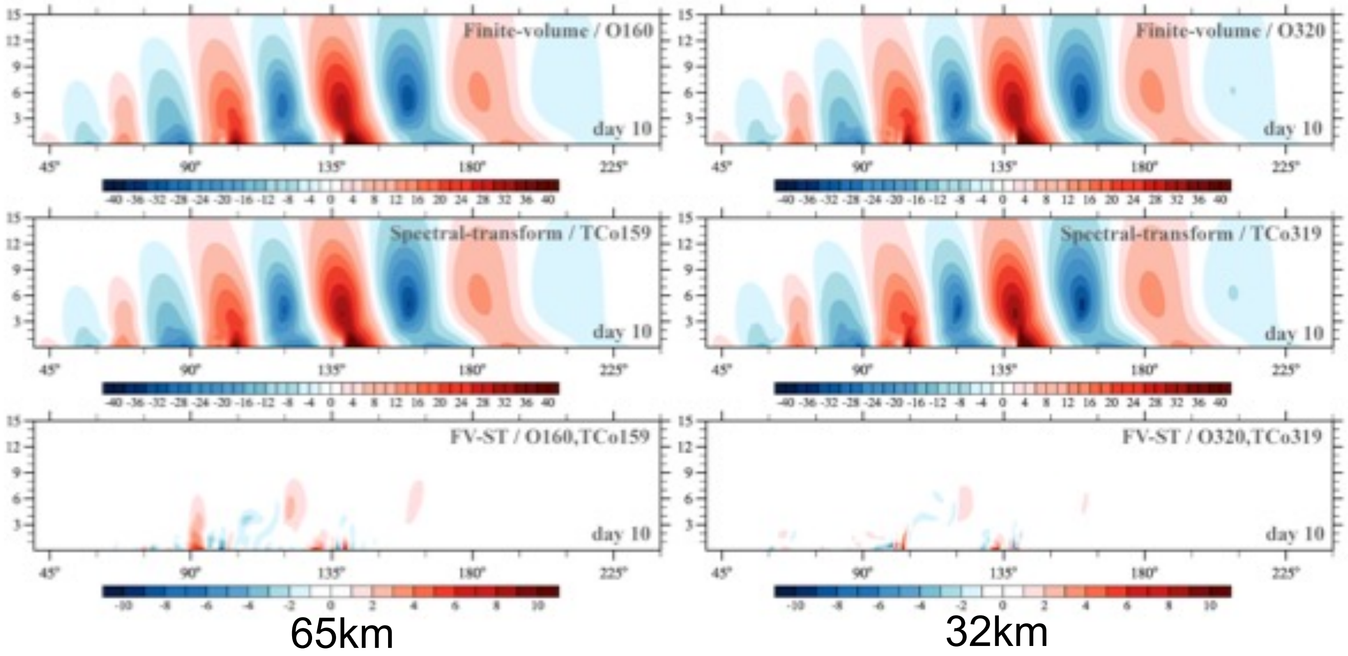

experimental setup following Ullrich et al. QJ 2012

FVM comparison to hydrostatic IFS-ST: dry adiabatic dynamics

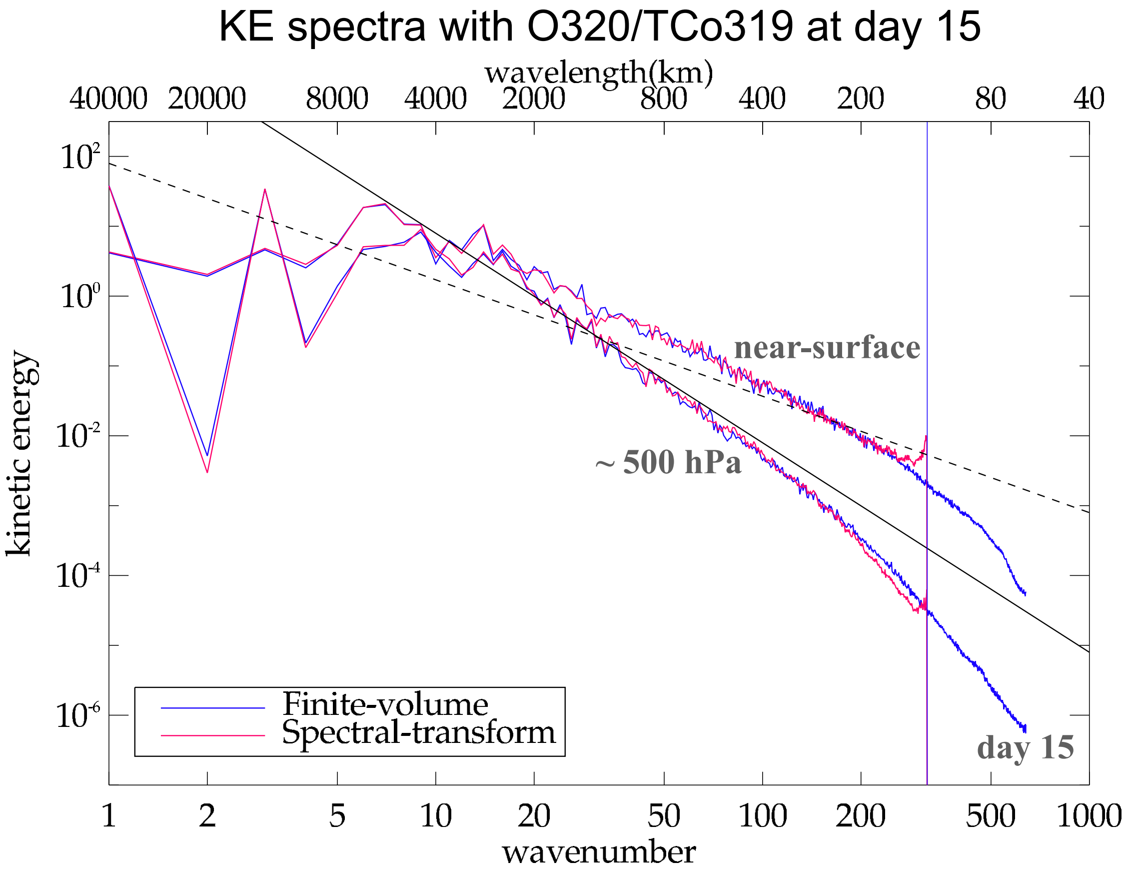

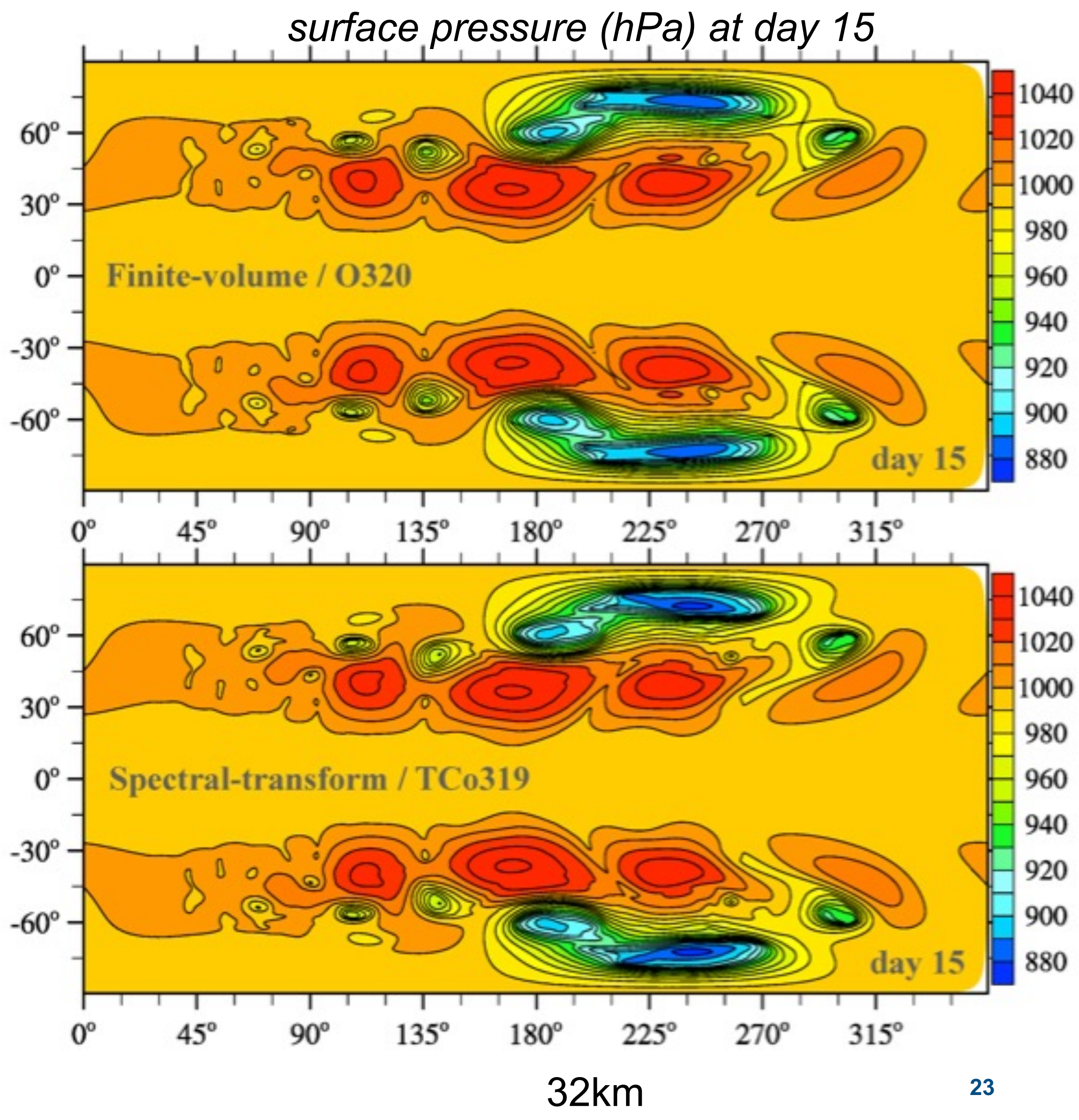

Second-order finite-volume provides essentially the same solution-quality than spectral-transform model for this test

ECMWF

Snapshot of computational efficiency: FVM vs IFS-ST

- Dry baroclinic instability experiments in identical configuration O1280/TCo1279 (9km) with L137
- Time steps of IFS-FVM were a factor of 6-7 smaller than IFS-ST

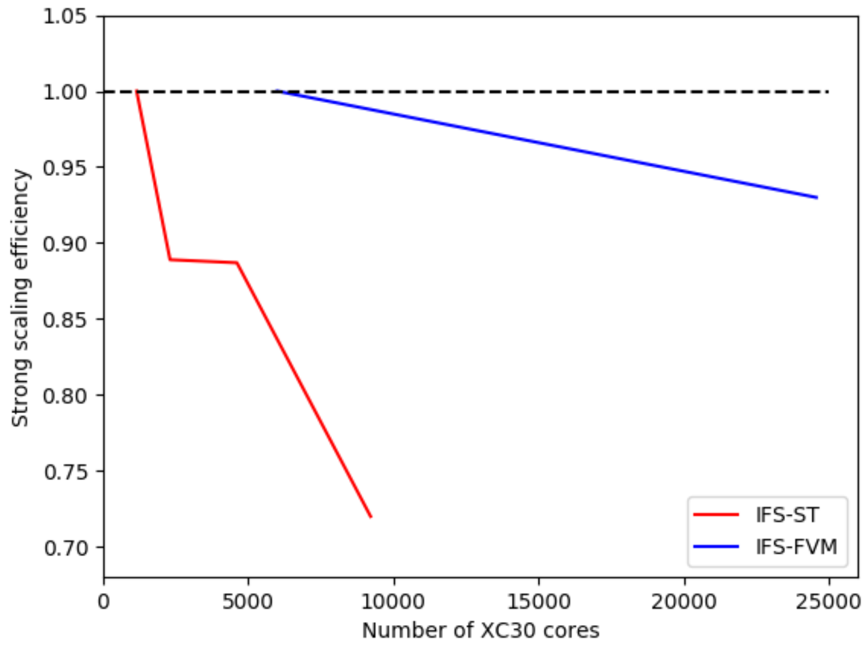

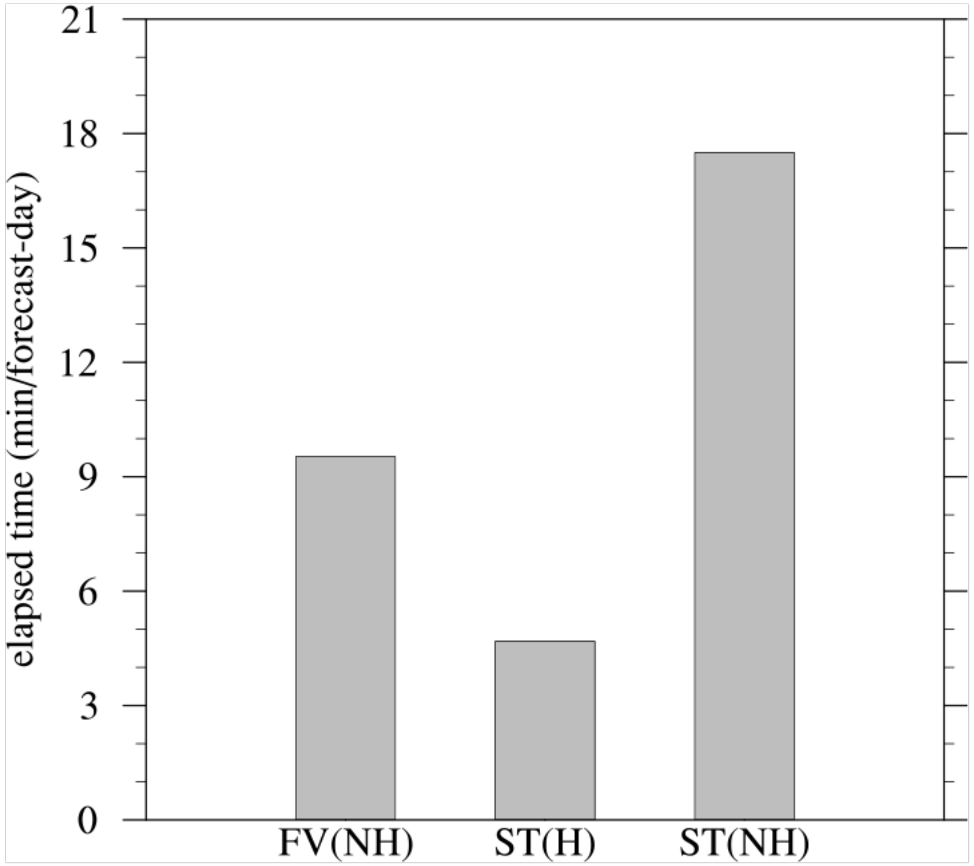

O1280/TCo1279 with L137 dry dycore on 350 nodes of ECMWF's Cray XC40

Comparison study on latest GPU hardware in prep!

Octahedral and HEALPix meshes with FVM

Octahedral O400 example for baroclinic instability benchmark

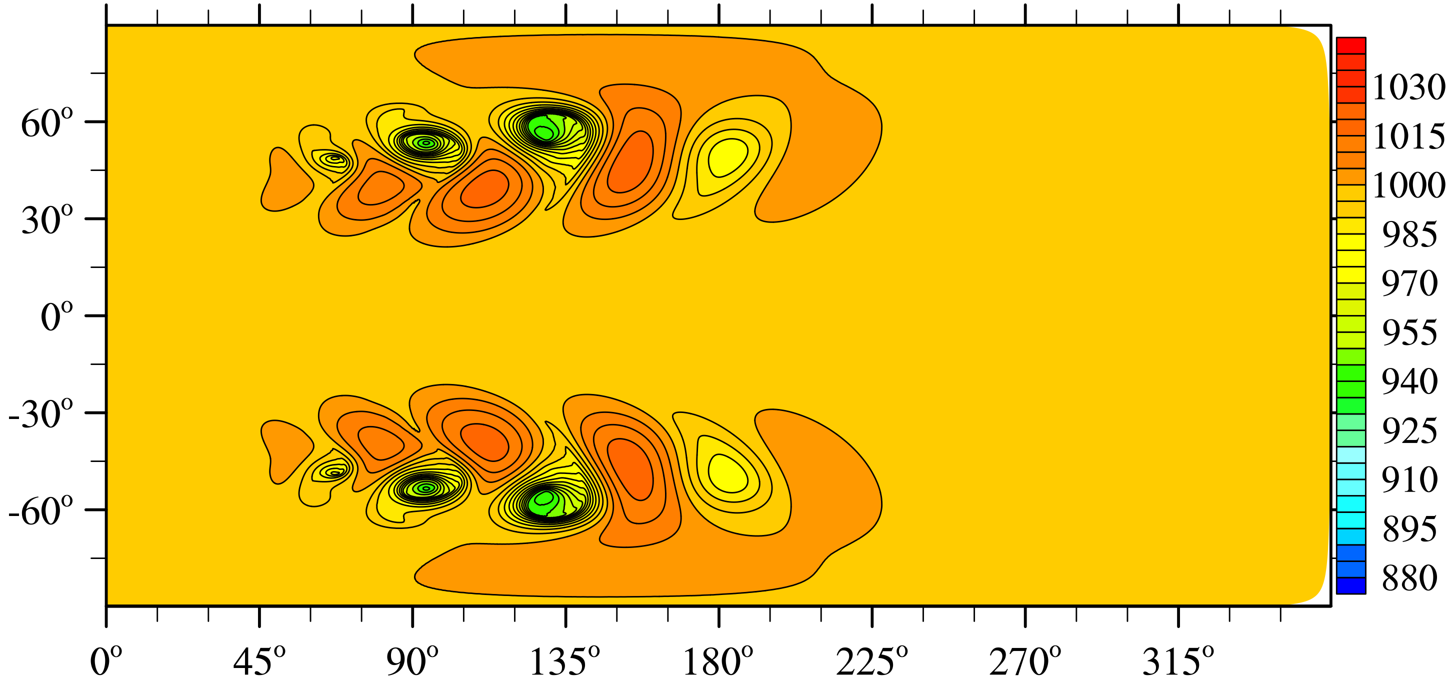

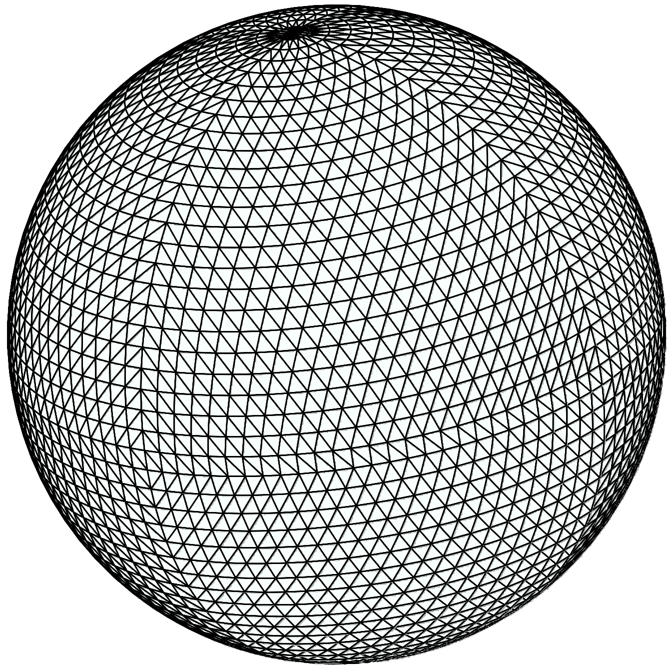

O24

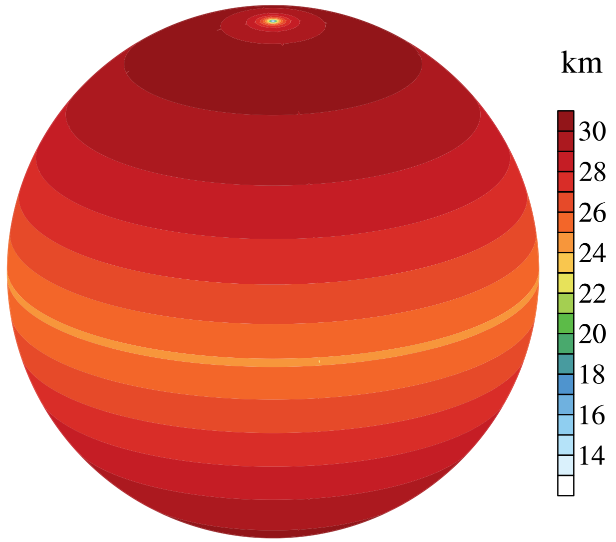

O400

Octahedral and HEALPix meshes with FVM

HEALPix H240 example for baroclinic instability benchmark

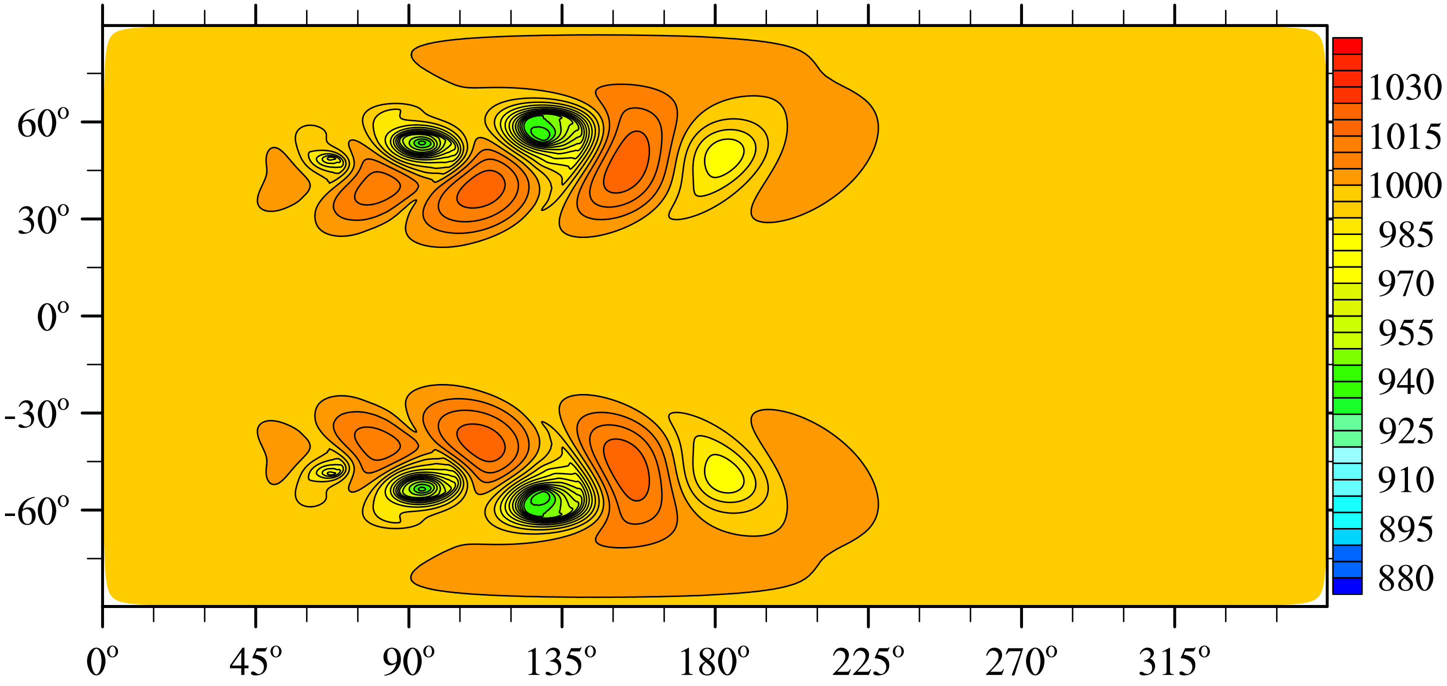

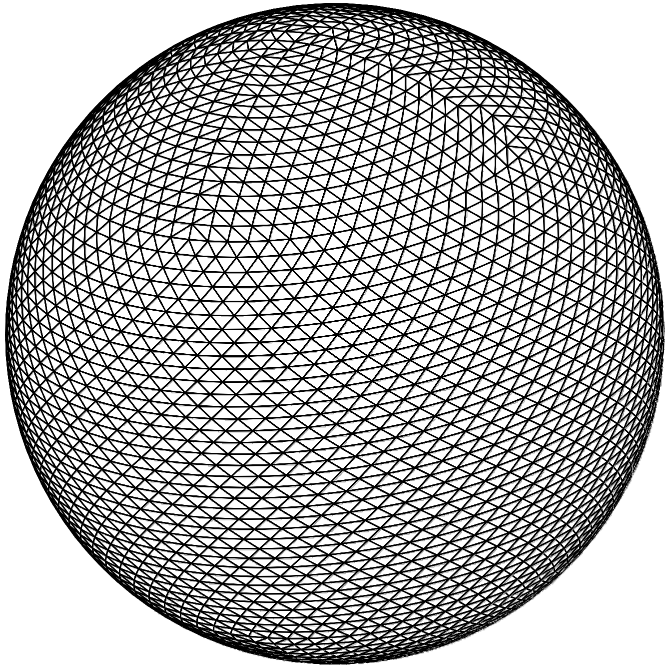

H18

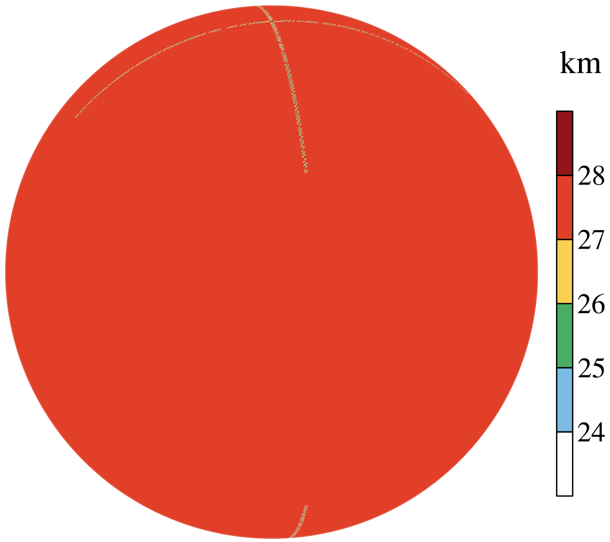

H240

Octahedral and HEALPix meshes with FVM

HEALPix H240 example for baroclinic instability benchmark

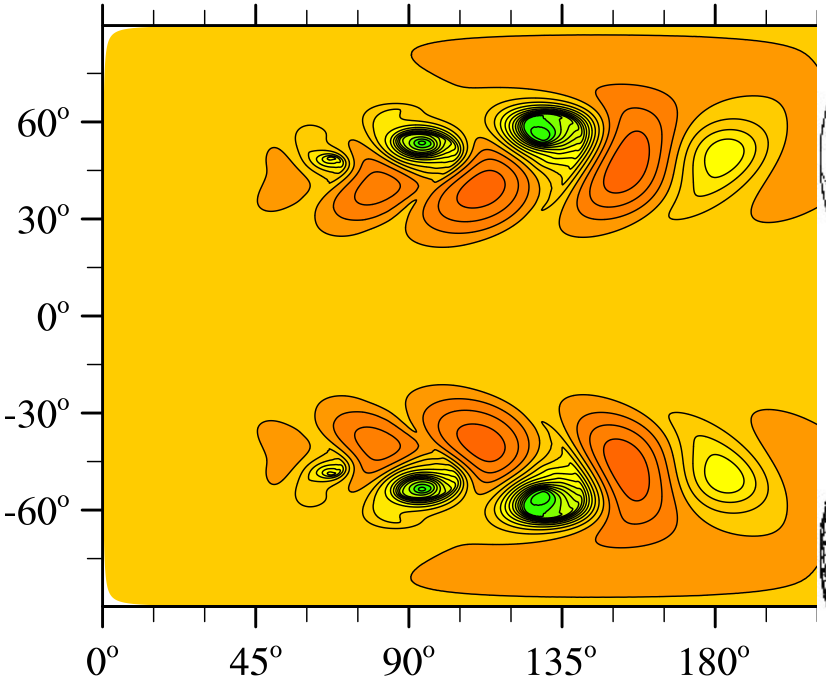

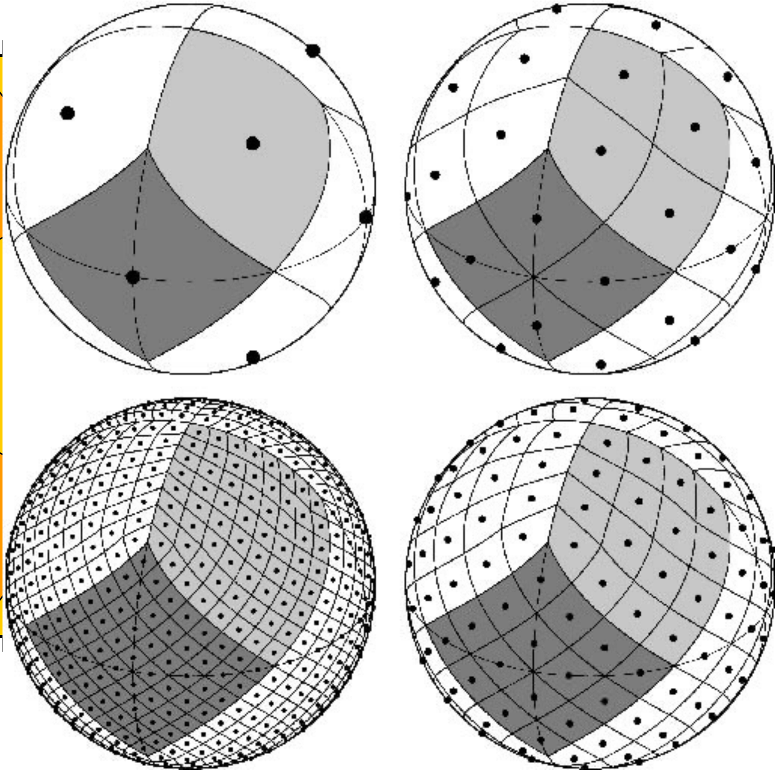

https://healpix.sourceforge.io/

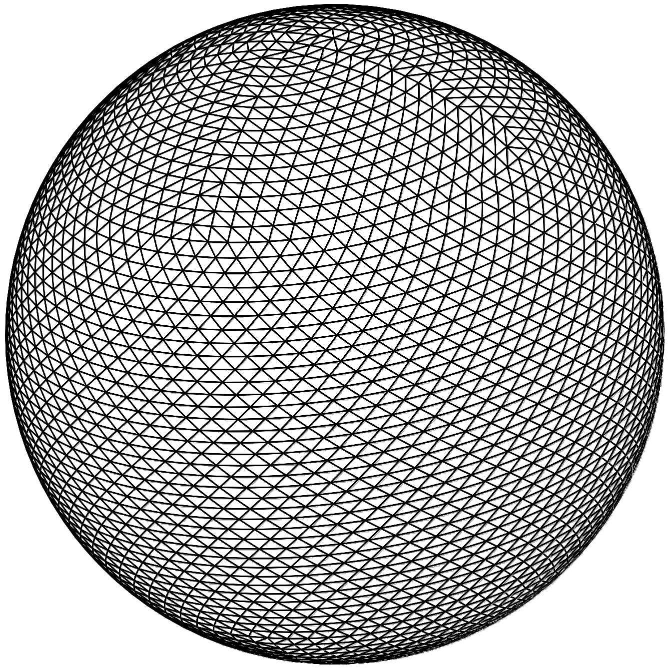

H18

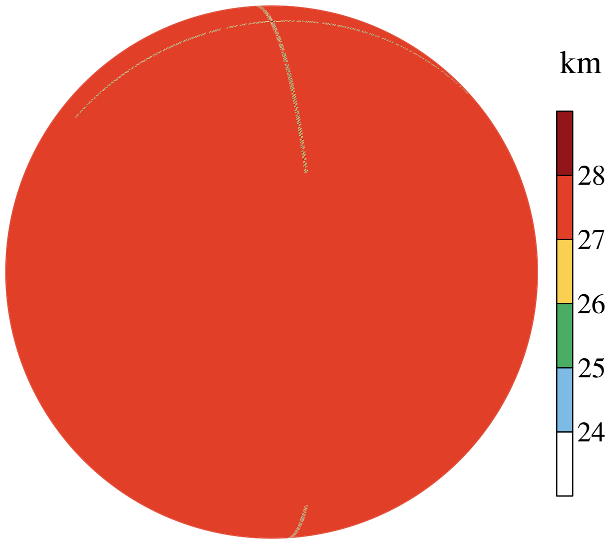

H240

Stratified flow past Schär mountain in small-planet configuration

MPAS

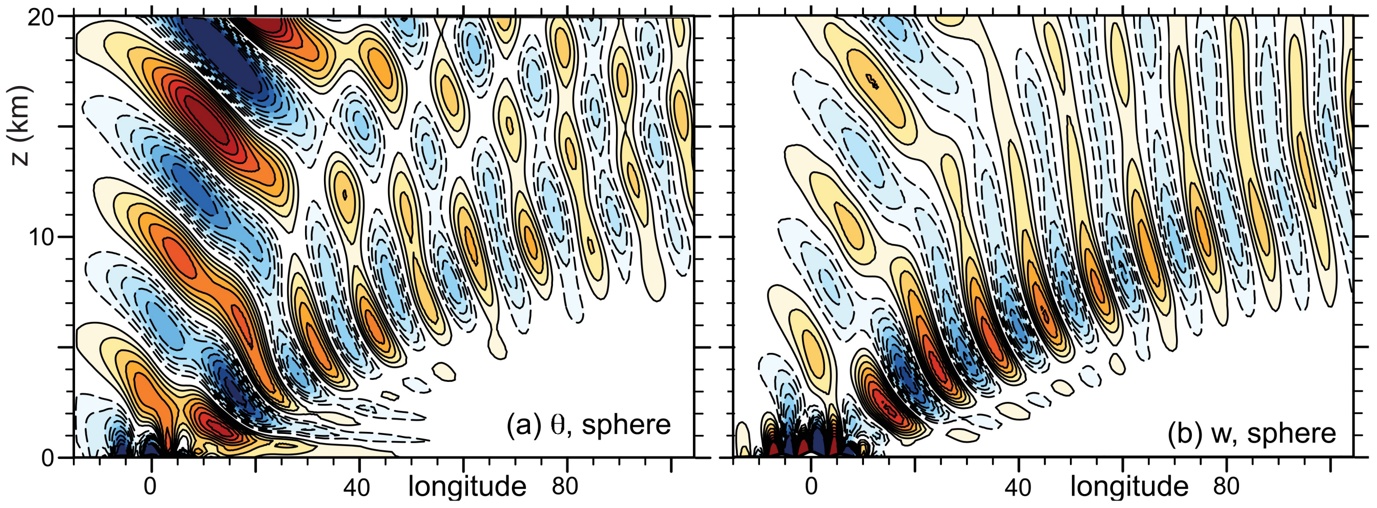

MPAS results from
Klemp et al. JAMES 2015

FVM

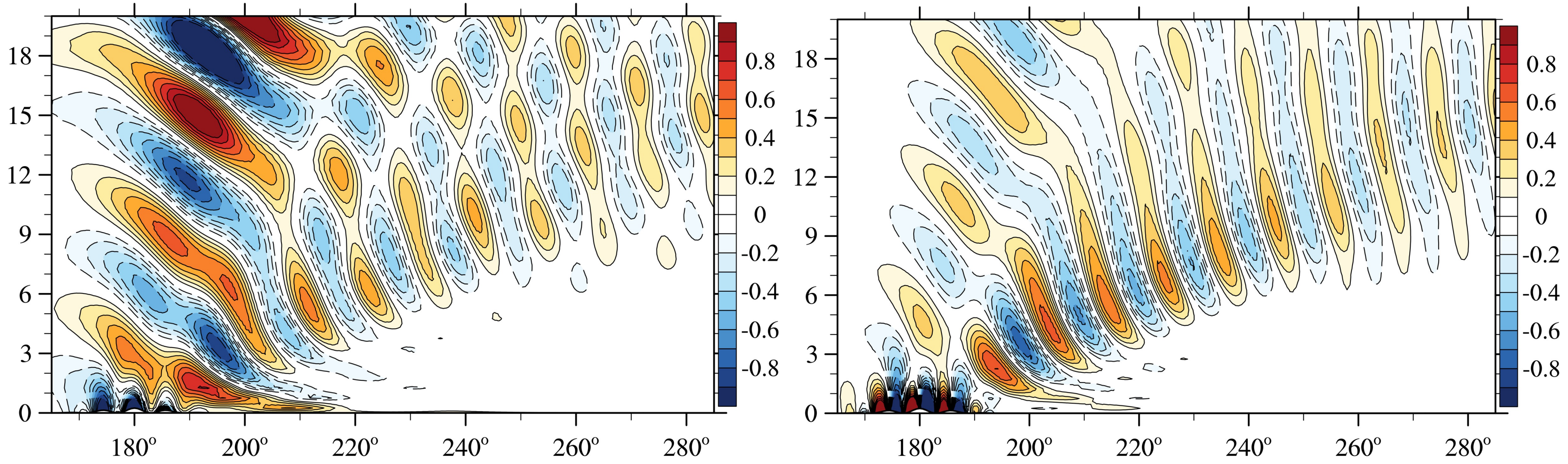

solution after 2hrs

Stratified flow past steep orography in small-planet configuration

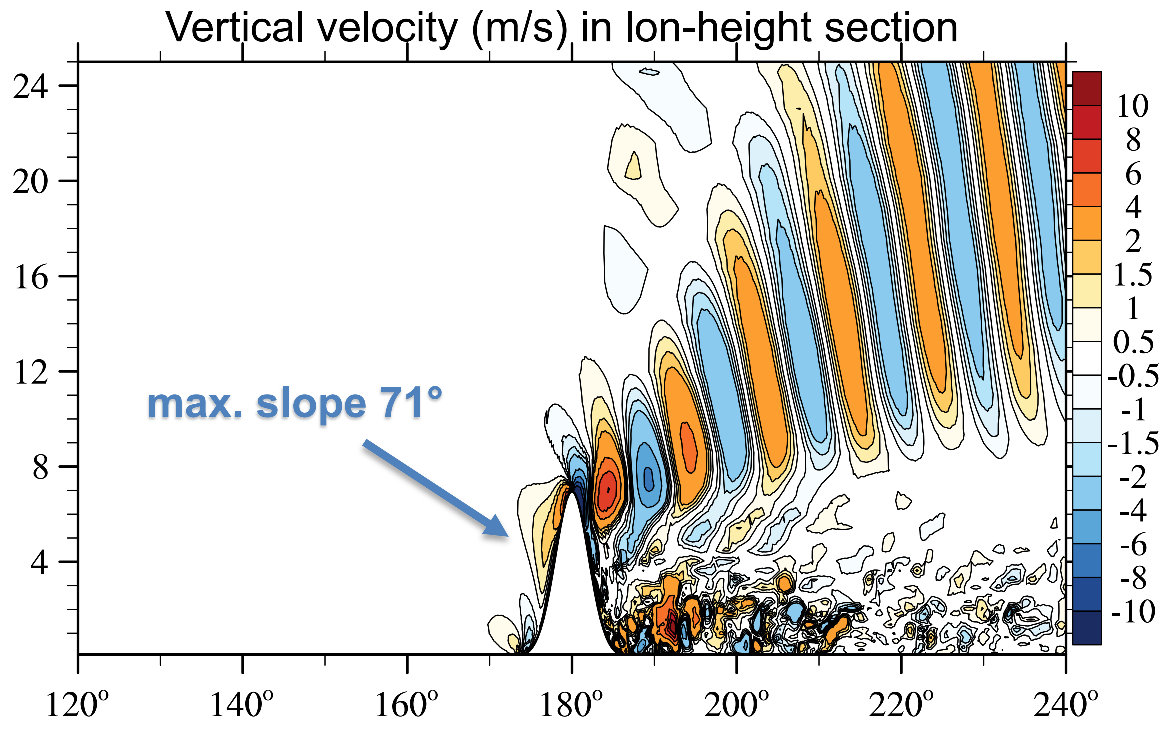

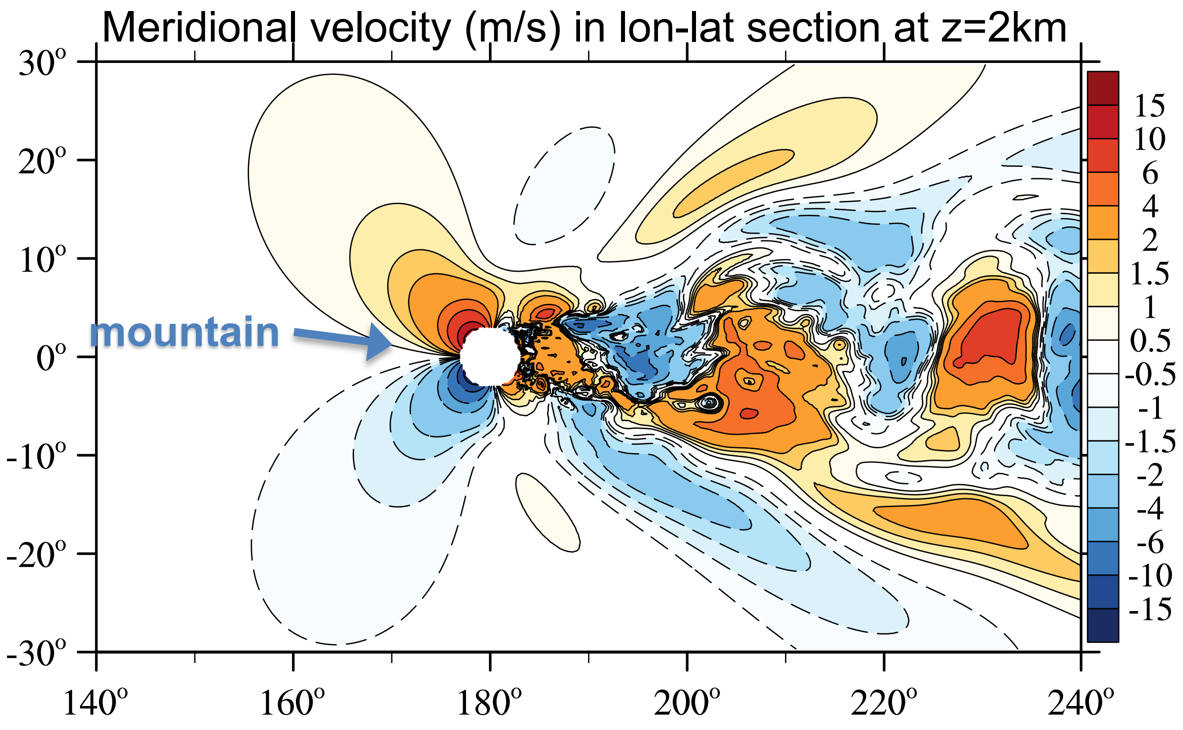

Experimental setup following Zängl MWR 2012

→ IFS-FVM robust wrt very steep slopes of orography

DCMIP2016 dynamical core intercomparison: splitting supercell

vertical velocity (m/s) in lon-lat section at z=5km

rain water (g/kg) in lon-lat section at z=5km

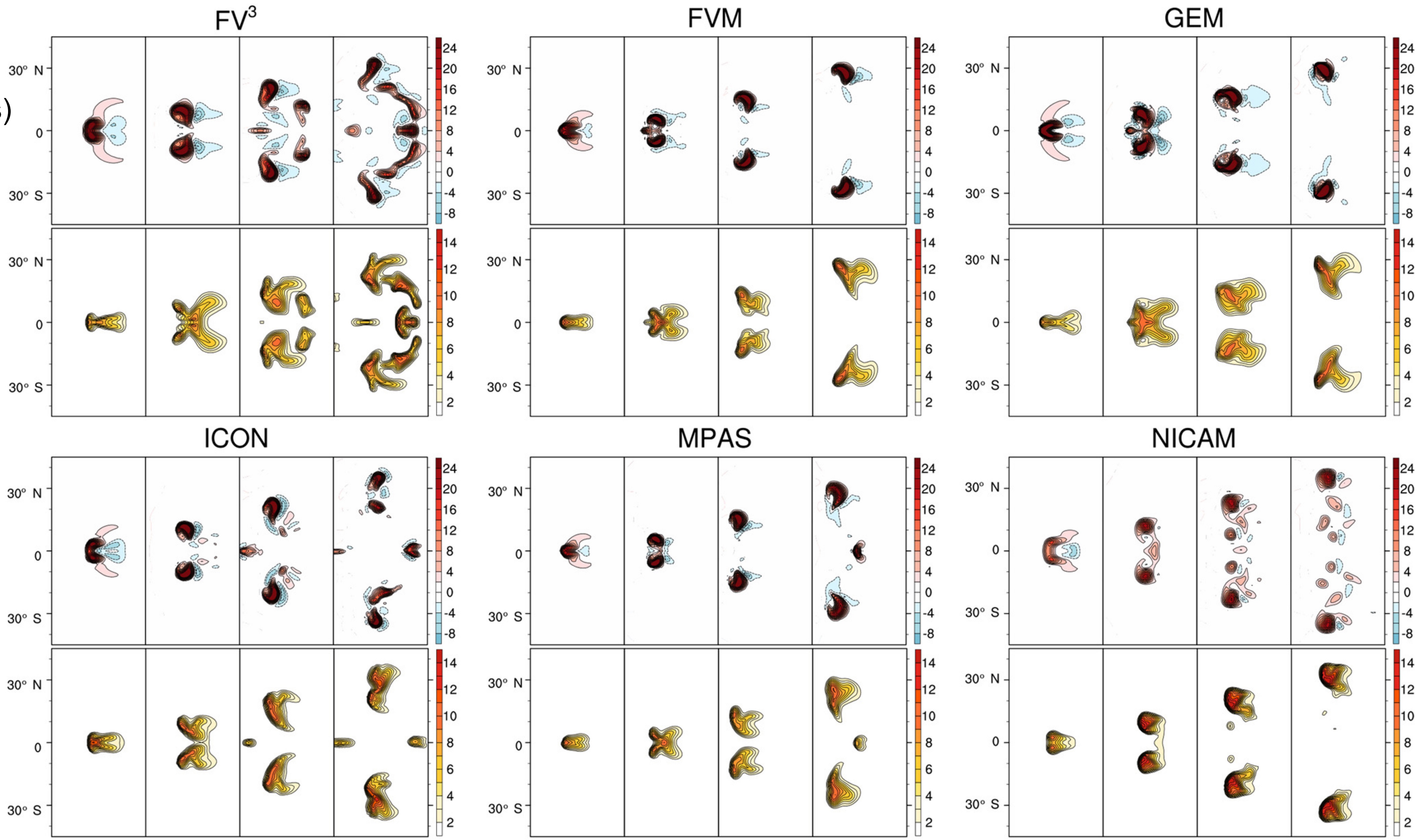

temporal evolution (panels are at 0.5,1.0,1.5, 2.0 h)

Zarzycki et al. GMD 2019

DCMIP2016 dynamical core intercomparison: splitting supercell

vertical velocity (m/s) in lon-lat section at z=5km

rain water (g/kg) in lon-lat section at z=5km

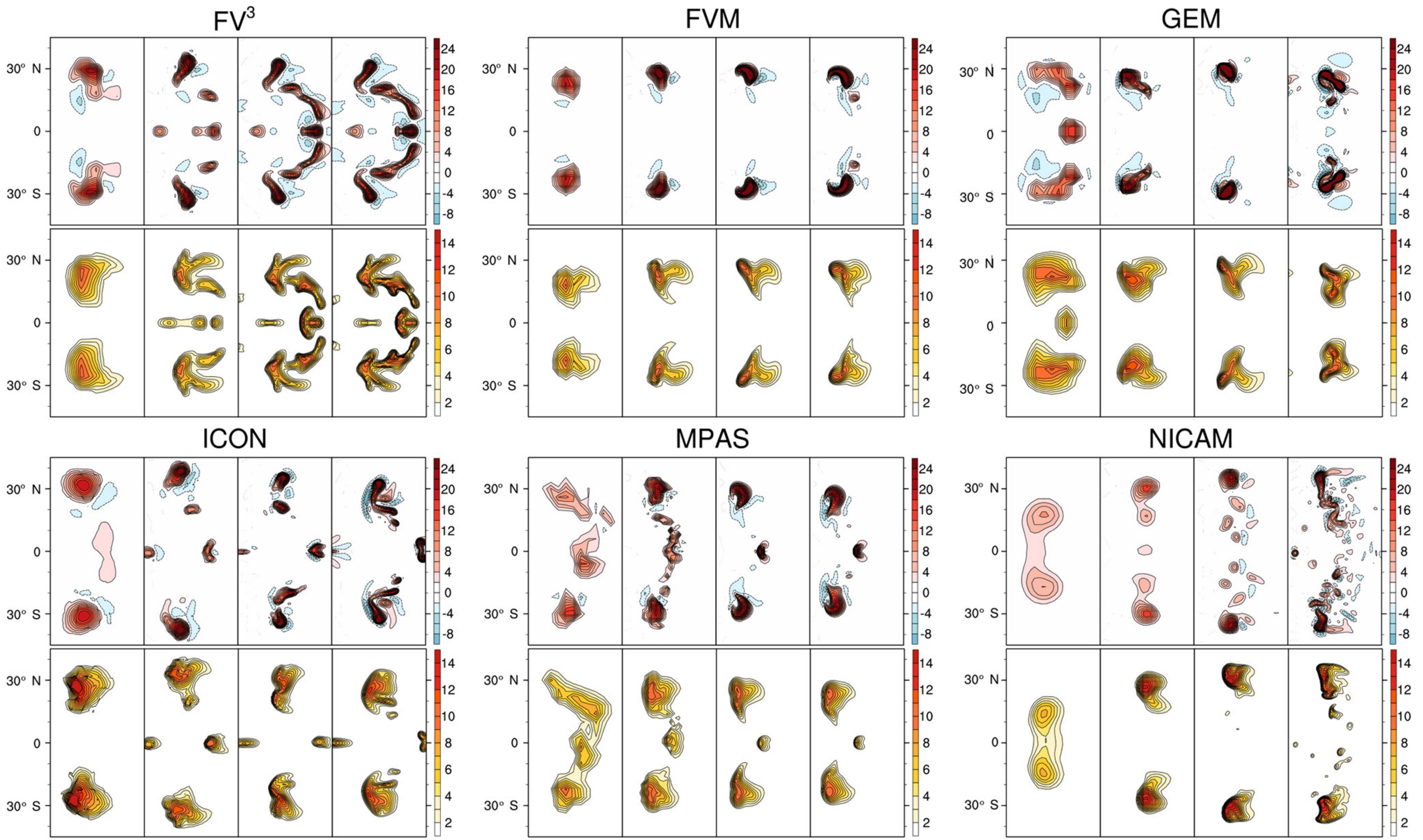

final 2h result as various grid spacing (panels are at 4, 2, 1, 0.5 km)

Zarzycki et al. GMD 2019

DCMIP2016 dynamical core intercomparison: splitting supercell

Zarzycki et al. GMD 2019

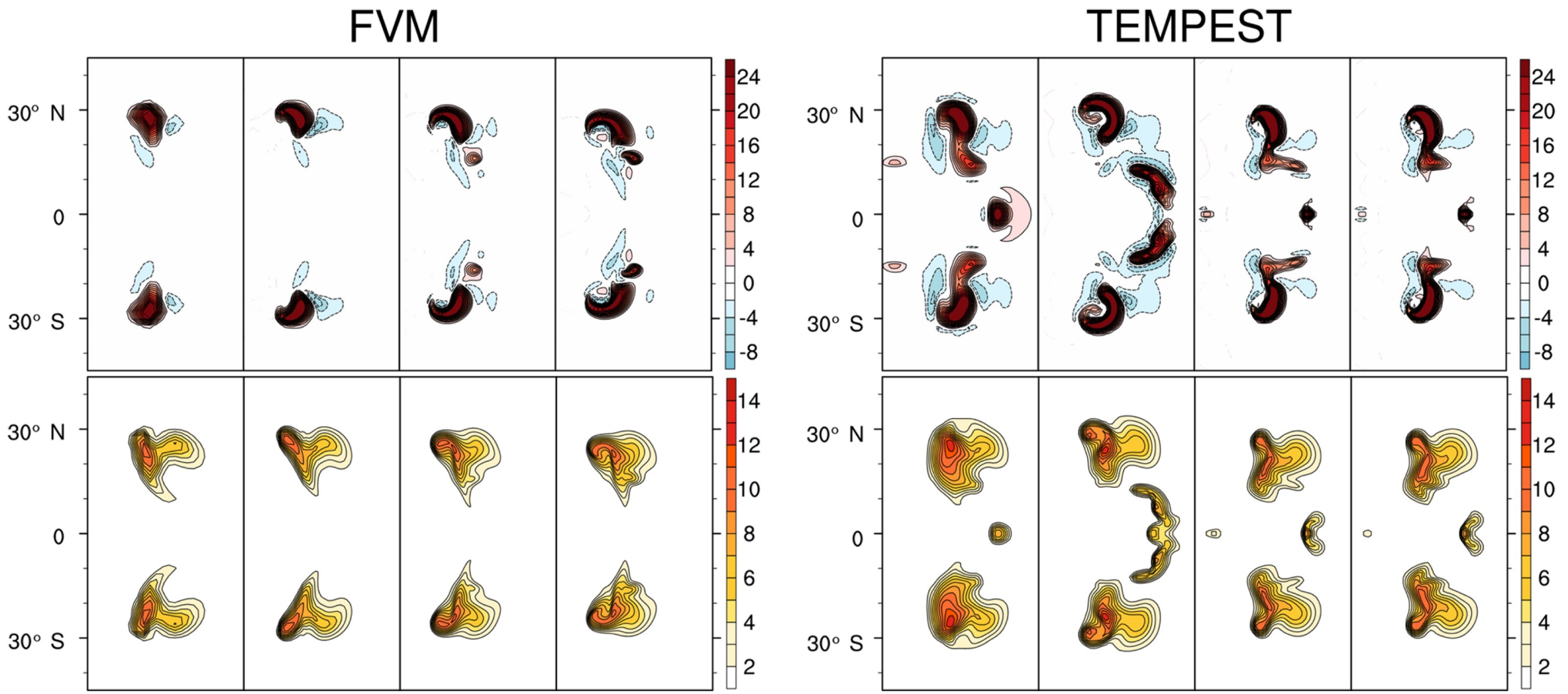

final 2h result as various grid spacings (panels are at 2, 1, 0.5, 0.25 km)

→ FVM uses second-order Finite-Volume method

→ TEMPEST uses higher-order Spectral-Element methods

$$\mathrm{IKE}(t) = \frac{1}{2}\int_0^{z_t}\int_0^{A_e} \rho\left(u'^2 + v'^2 + w'^2\right)\mathrm{d}A\mathrm{d}z$$

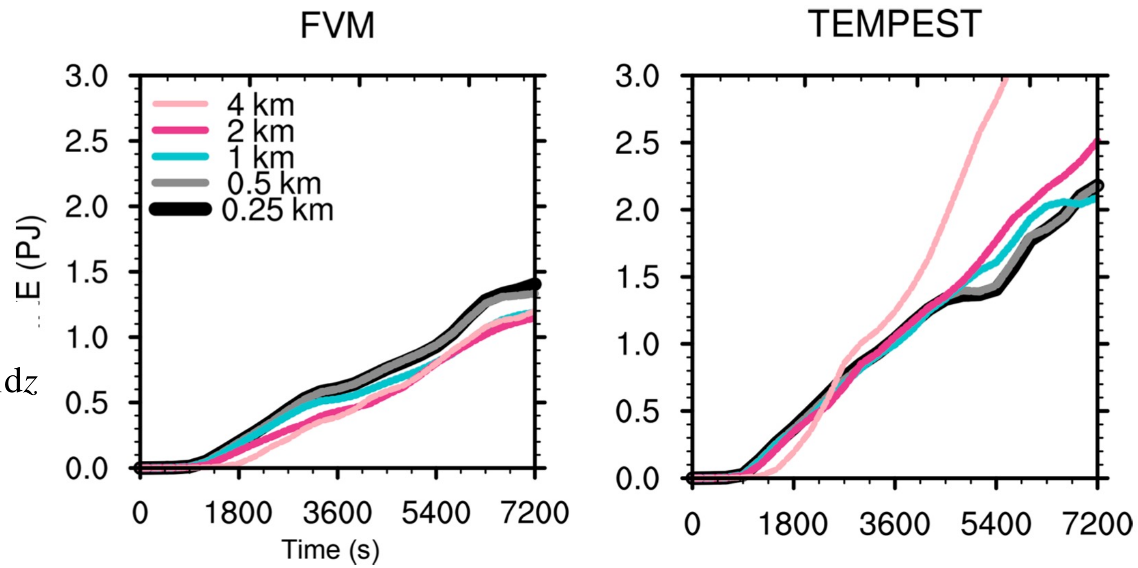

DCMIP2016 dynamical core intercomparison: tropical cyclone

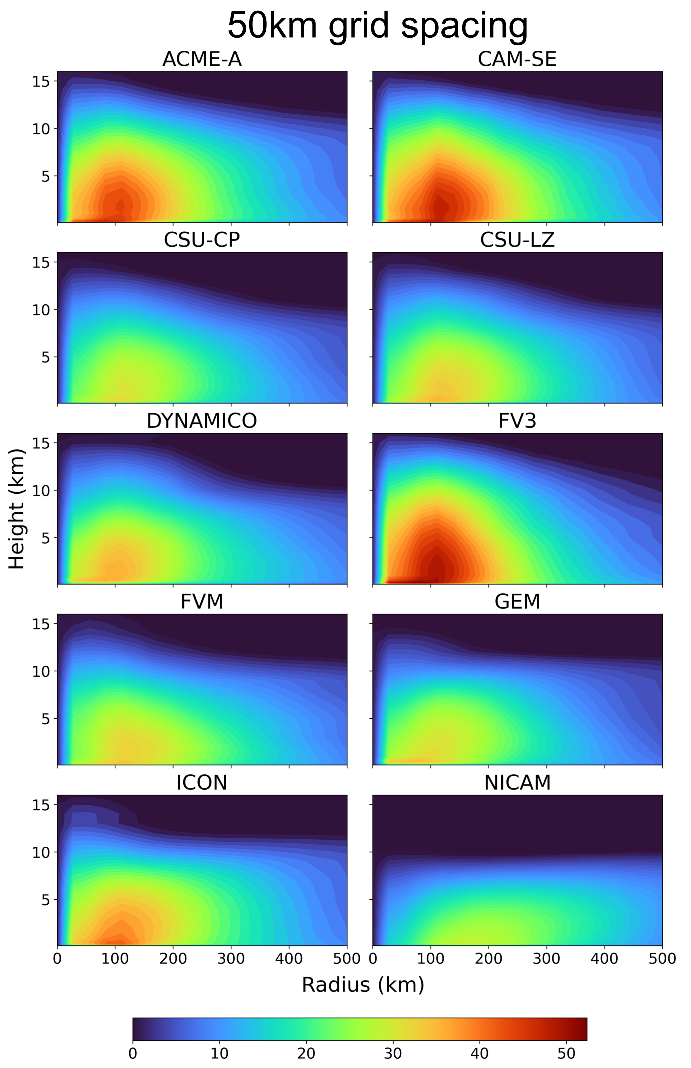

Figure 4. Azimuthally averaged vertical wind composite of the simulated TCs from days 4–10 of the 50 km simulation.

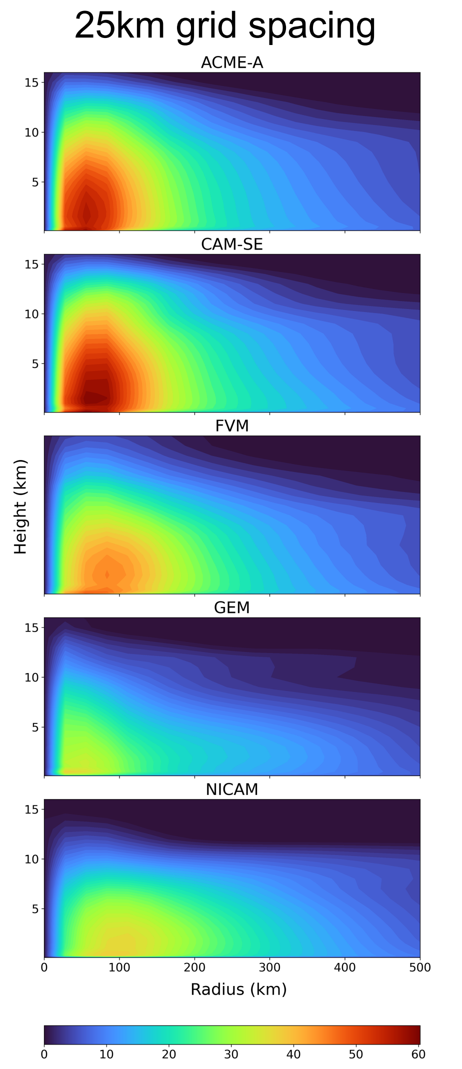

Figure 8. Azimuthally averaged vertical wind composite of the simulated TCs from days 4–10 of the 25 km simulation.

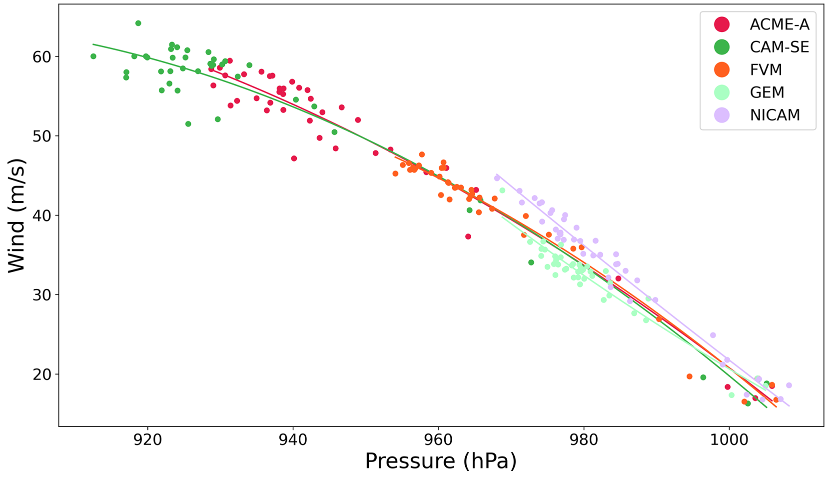

Figure 6. Wind–pressure relationship in the simulated TCs at all time steps for 25 km simulations of participating models.

Willson et al. GMD 2024

DCMIP2016 dynamical core intercomparison: tropical cyclone

50km grid spacing

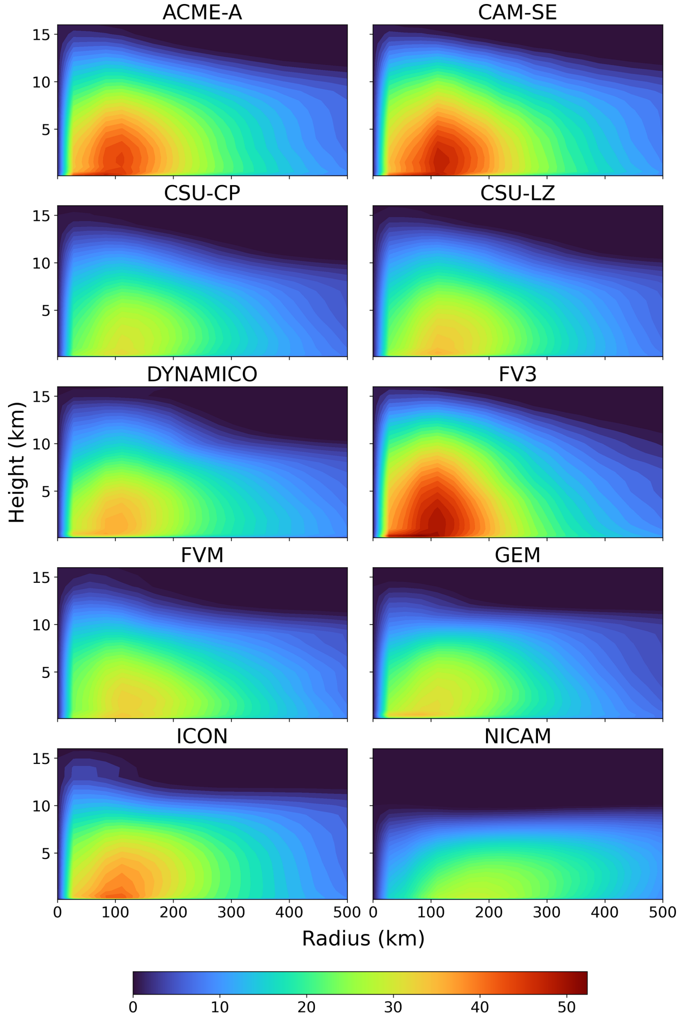

Figure 4. Azimuthally averaged vertical wind composite of the simulated TCs from days 4–10 of the 50 km simulation.

25km grid spacing

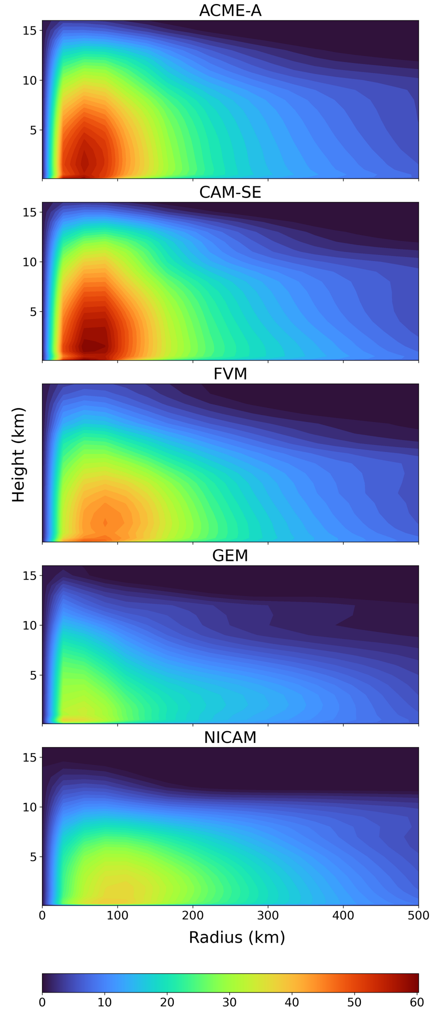

Figure 8. Azimuthally averaged vertical wind composite of the simulated TCs from days 4–10 of the 25 km simulation.

McTaggart-Cowan et al. 2024

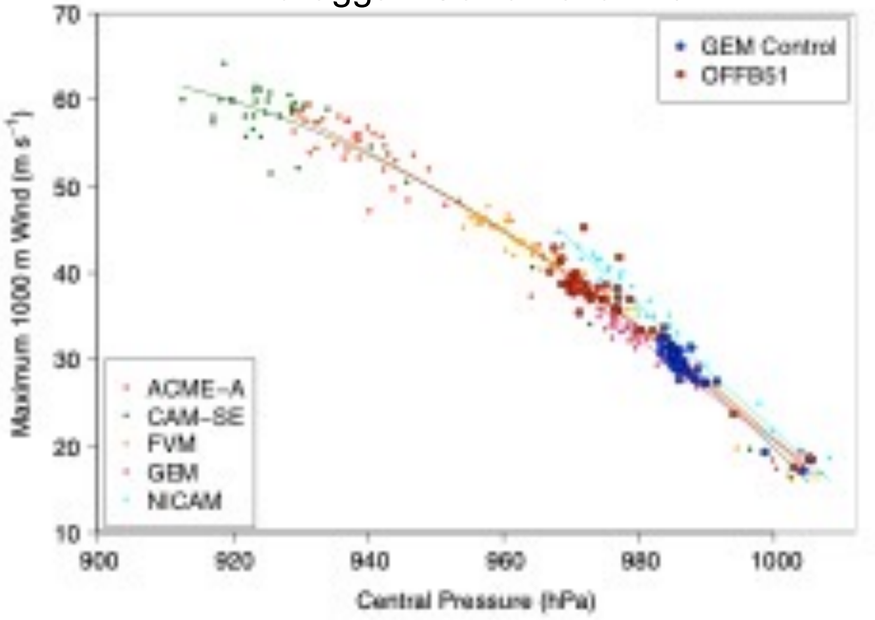

Willson et al. GMD 2024

FVM case study of Hurricane IRMA

- Major Hurricane of Category 5 in tropical Atlantic
- Formed 30 August 2017
- Dissipated 14 September 2017
- 285 km/h 1-minute sustained winds
- 914 hPa minimum MSLP
- Peak intensity on 5 September 2017
- Fourth-costliest tropical cyclone on record

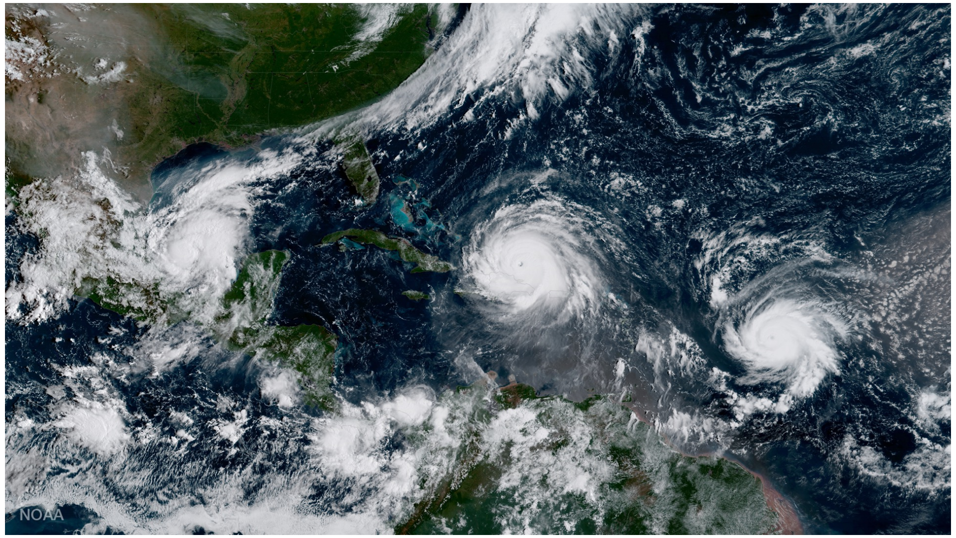

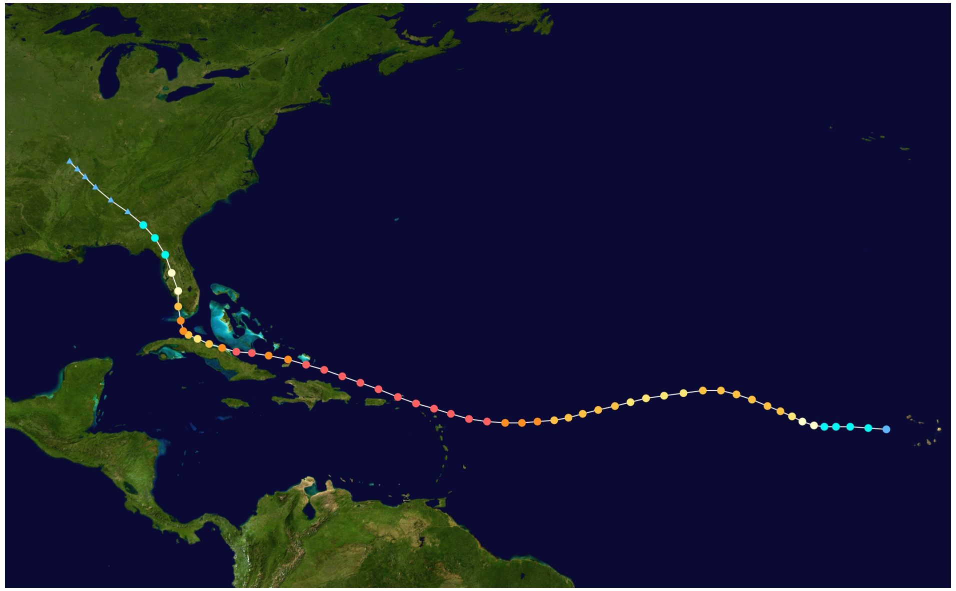

ECMWF

FVM forecast experiments of Hurricane IRMA

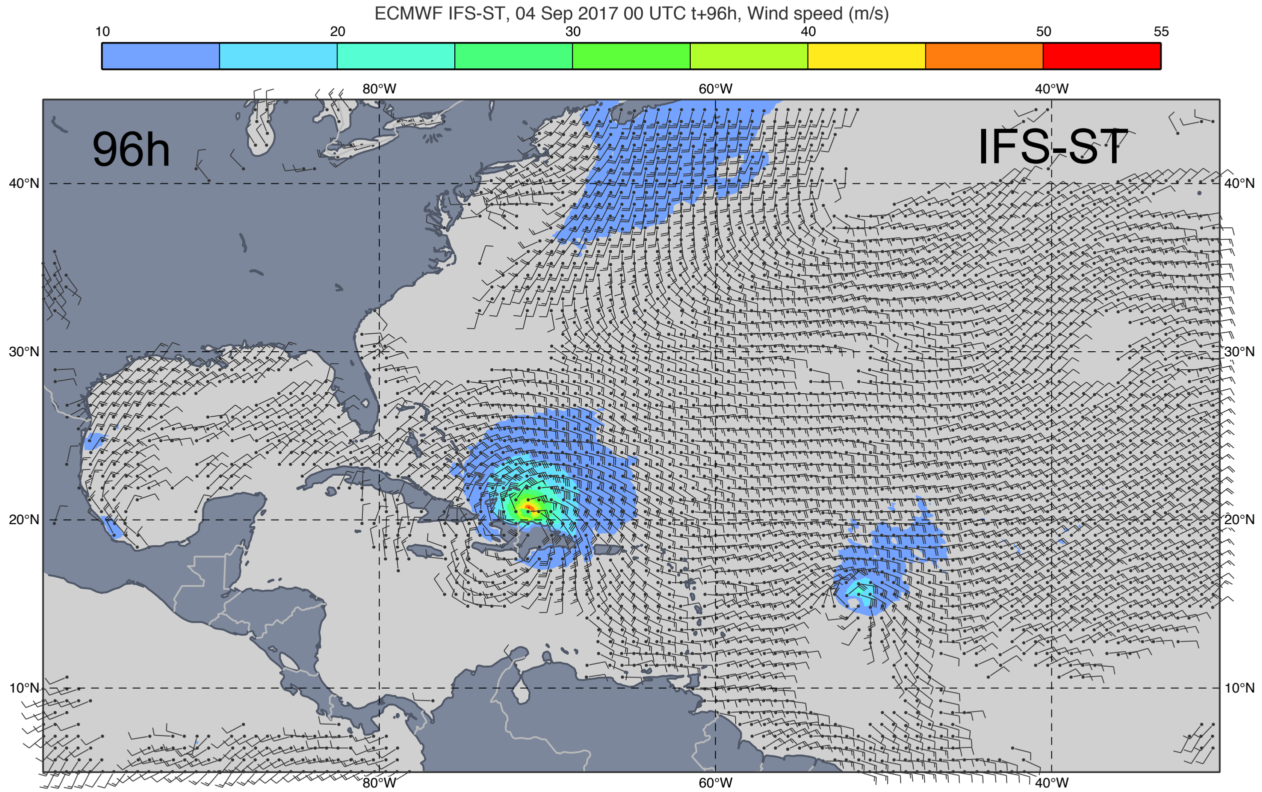

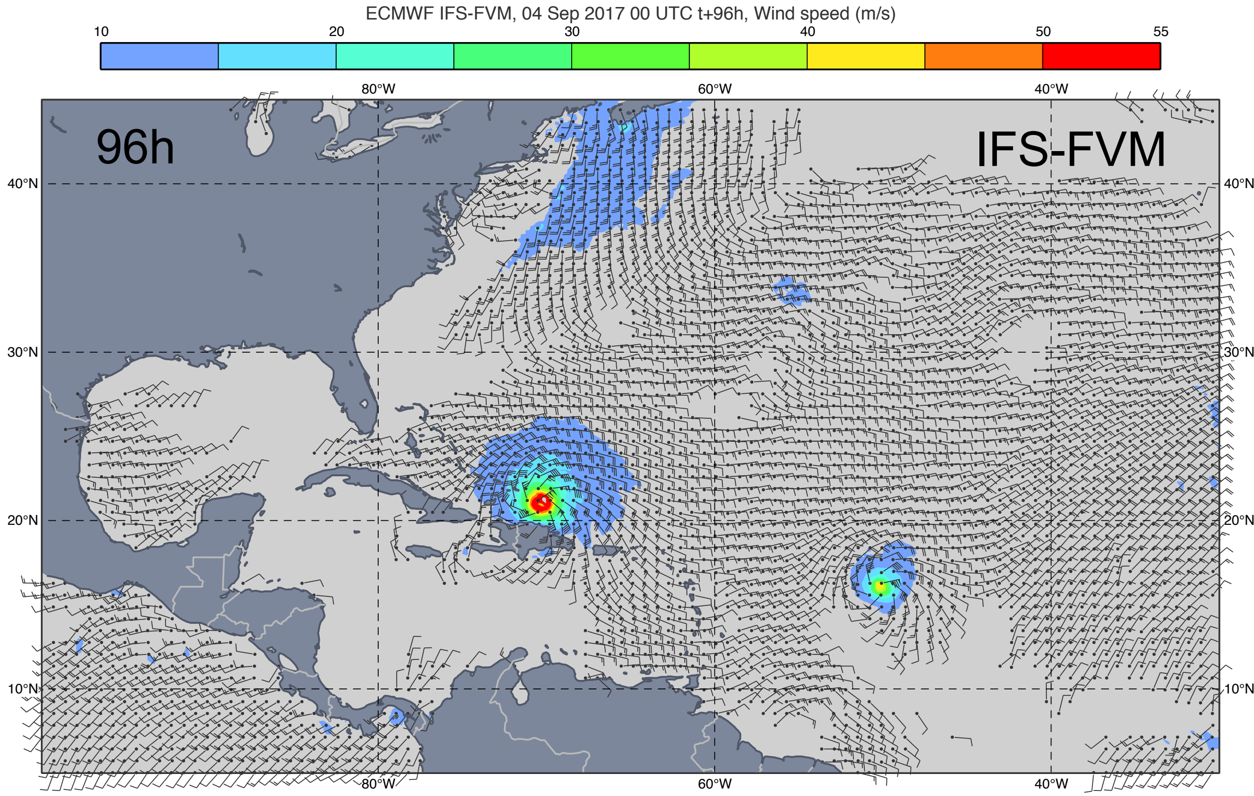

- Initialisation from IFS analysis 20170904 00 UTC
- O1280/TCo1279 corresponding to ~9 km nominal spacing, L62
- IFS CY43R3, uncoupled

ECMWF

FVM forecast experiments of Hurricane IRMA

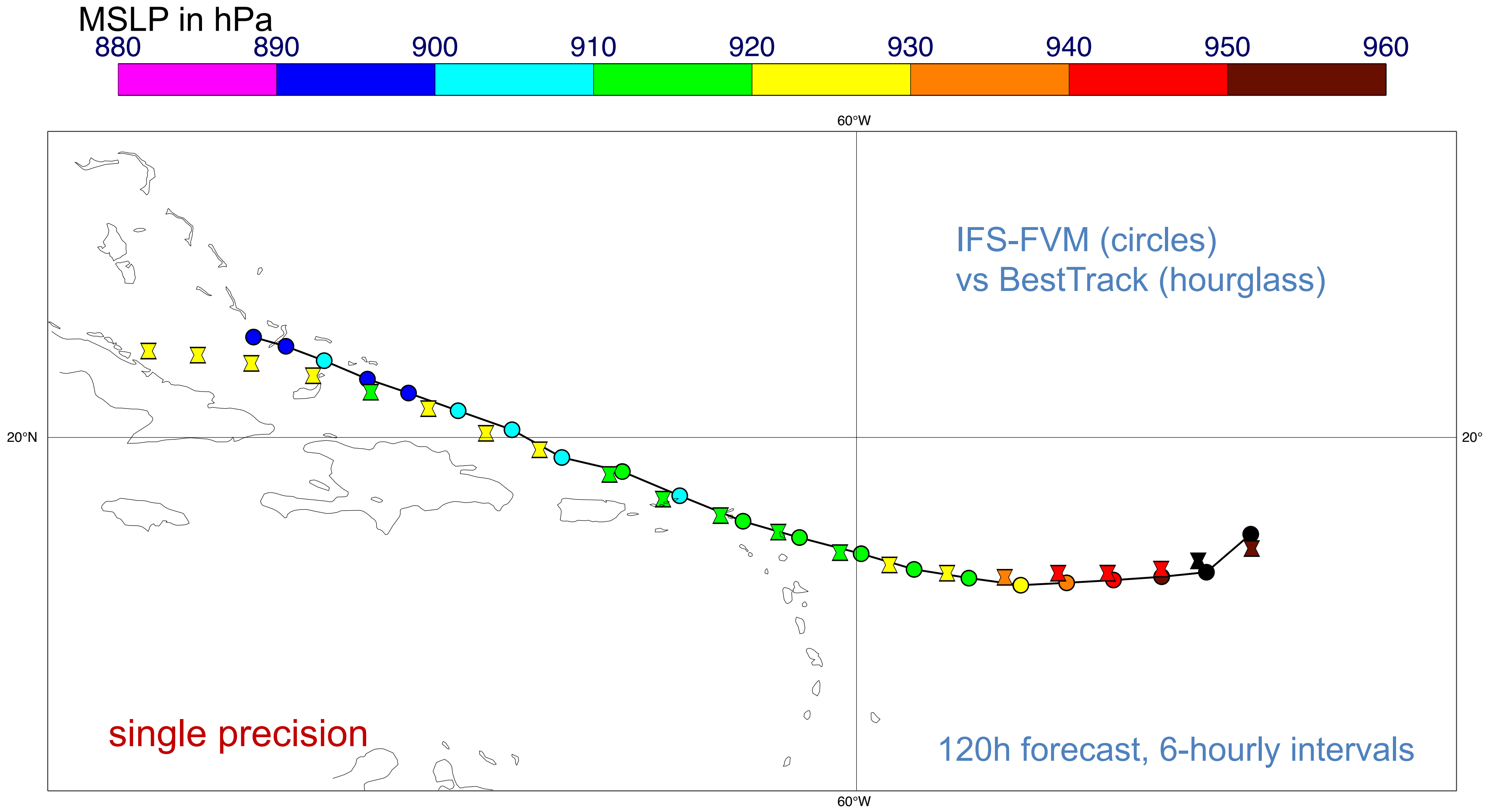

- Initialisation from IFS analysis 20170904 00 UTC
- O1280/TCo1279 corresponding to ~9 km nominal spacing, L62
- IFS CY43R3, uncoupled

Christian Kühnlein, Linus Magnusson

FVM forecast experiments of Hurricane IRMA

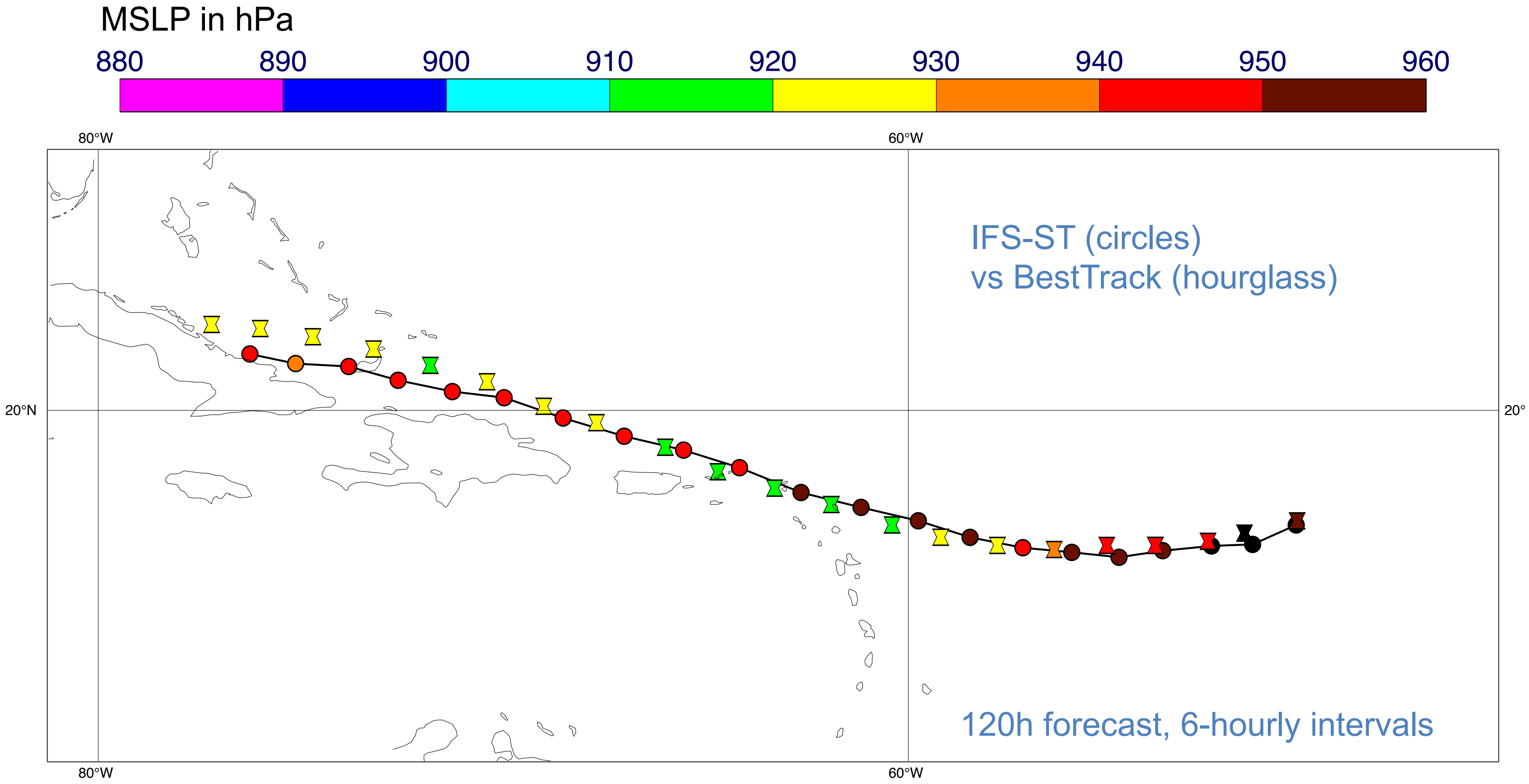

- Initialisation from IFS analysis 20170904 00 UTC
- O1280/TCo1279 corresponding to ~9 km nominal spacing, L62
- IFS CY43R3, uncoupled

ECMWF

Christian Kühnlein, Linus Magnusson

Relevance of nonhydrostatic effects for the supercell convective storm

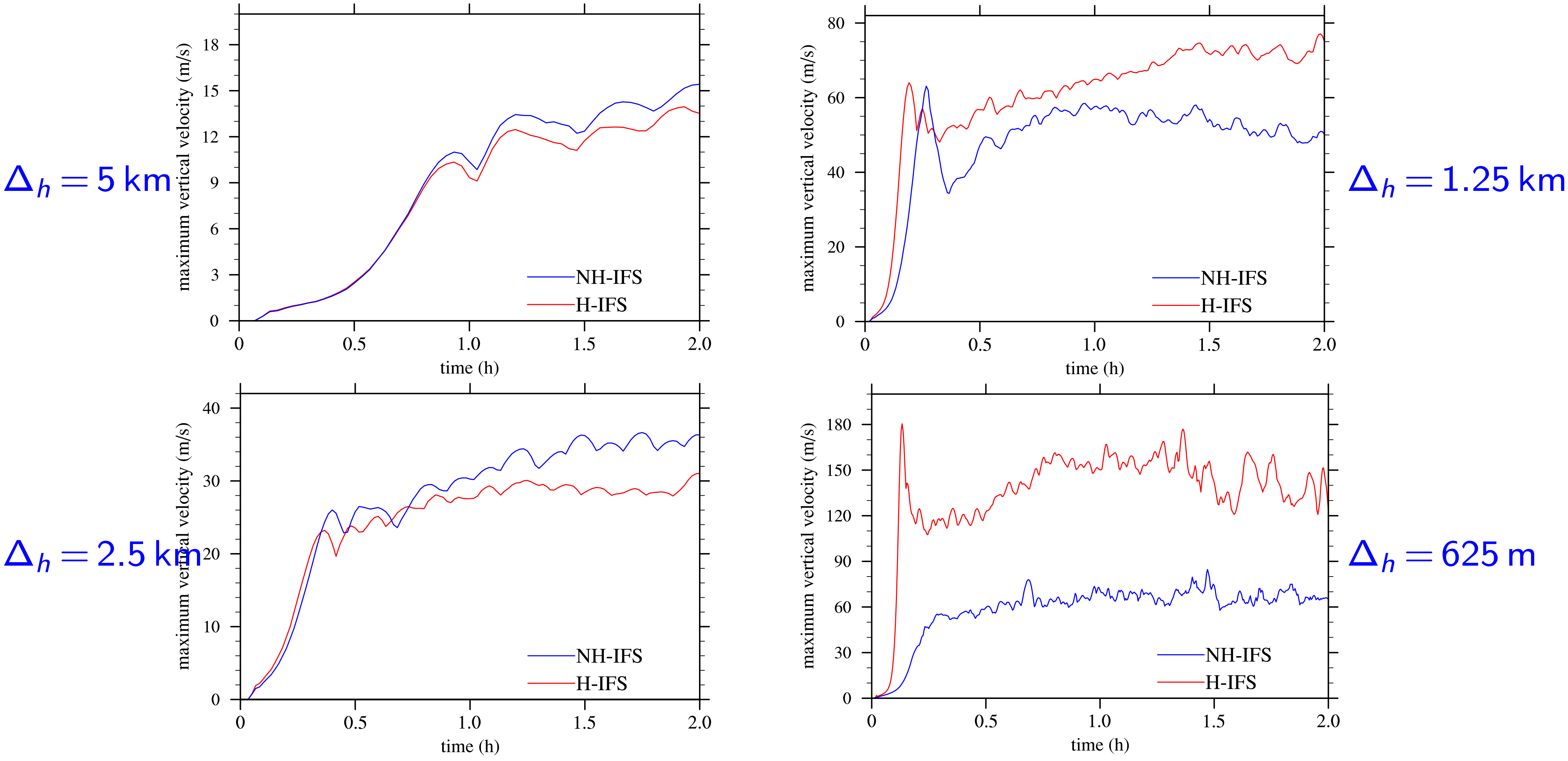

Relevance of nonhydrostatic effects for the supercell convective storm

$\Delta_h = 5$ km

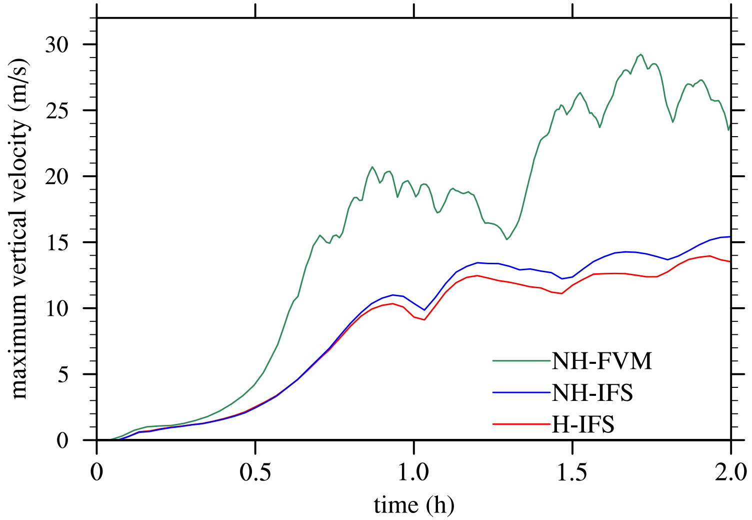

$\Delta_h = 1.25$ km

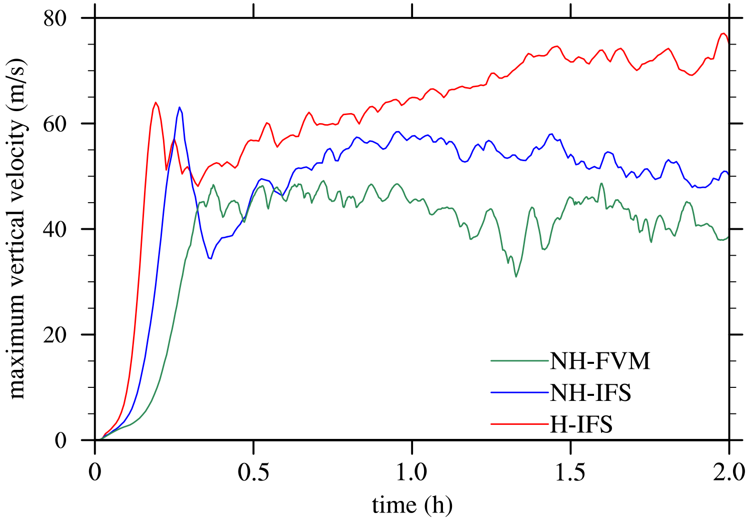

$\Delta_h = 2.5$ km

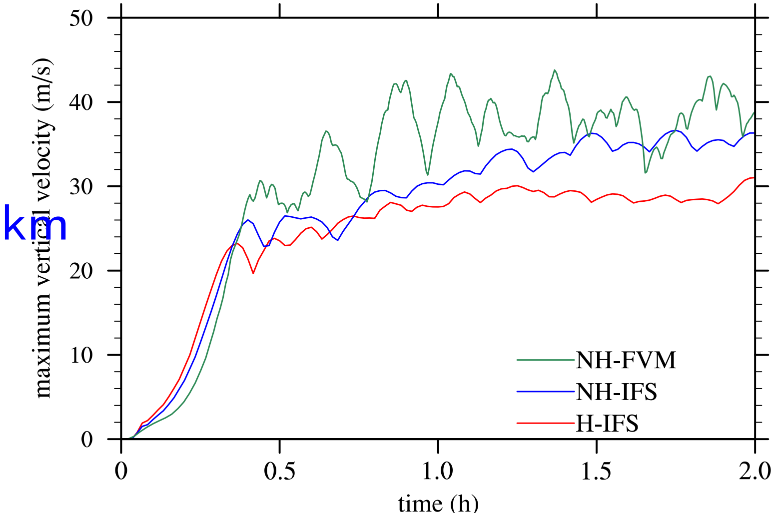

$\Delta_h = 625$ m

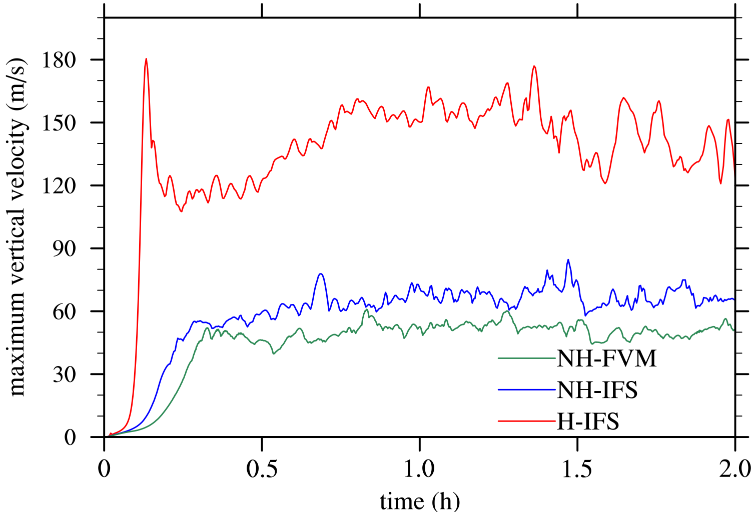

Single-precision implementation of FVM

MPI x OMP	72 x 18	144 x 9	144 x 18	288 x 9
SP	2315 s	2365 s	1260 s	1269 s
DP	3660 s	3634 s	2007 s	1926 s

- Runtimes for a O640/L62 4-day forecast using single- vs. double-precision on Cray XC40
- Configuration is for init date 22 May 2018 00 UTC, full IFS physics package, all parametrisations apart from radiation and non-orographic GW drag are called at every FVM time step here
- Radiation called every hour and run on the same O640 grid
- Convergence of the FVM preconditioned Krylov solver is essentially identical with SP and DP given typical thresholds

Single-precision implementation of FVM

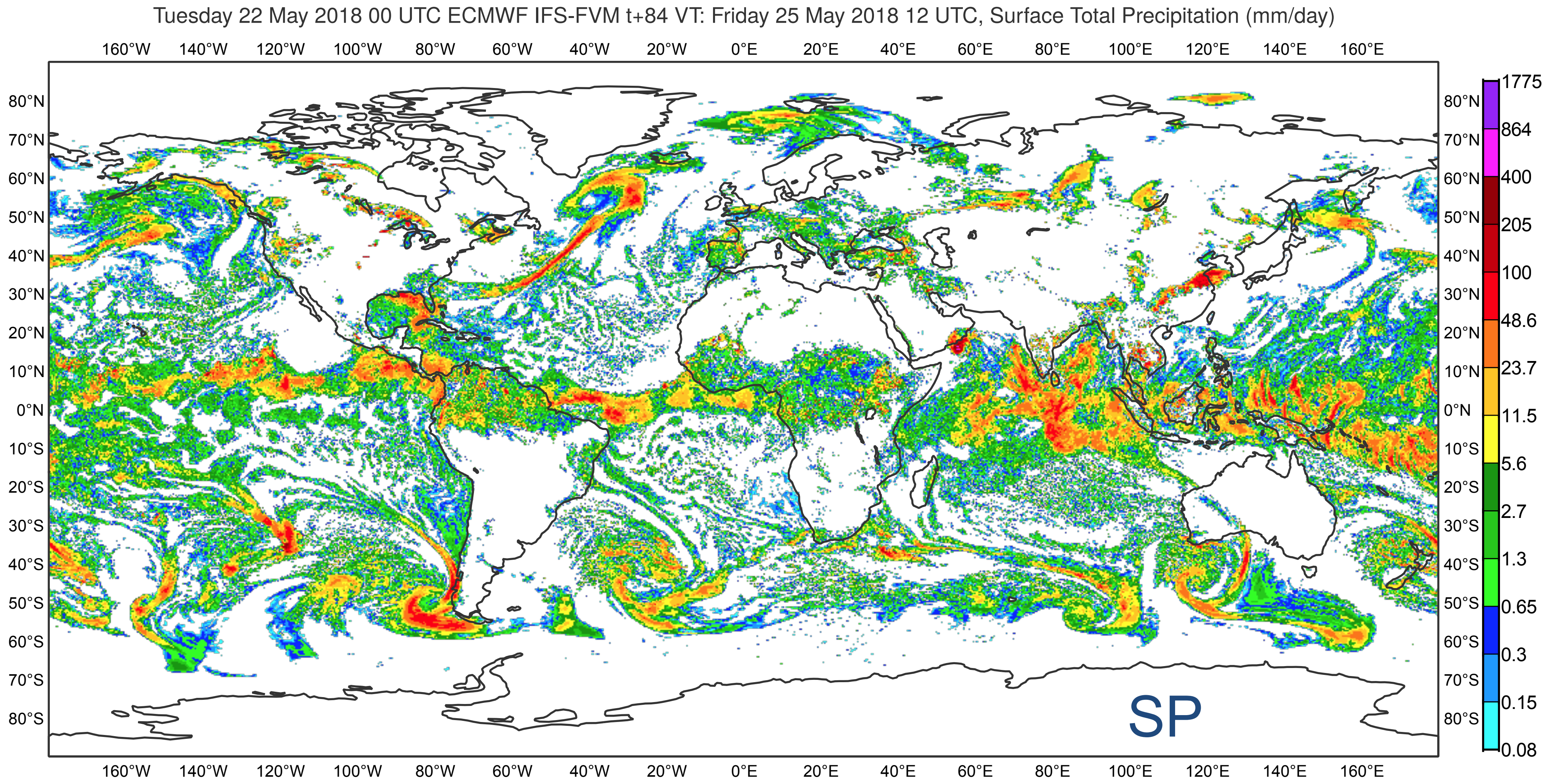

Single-precision implementation of FVM

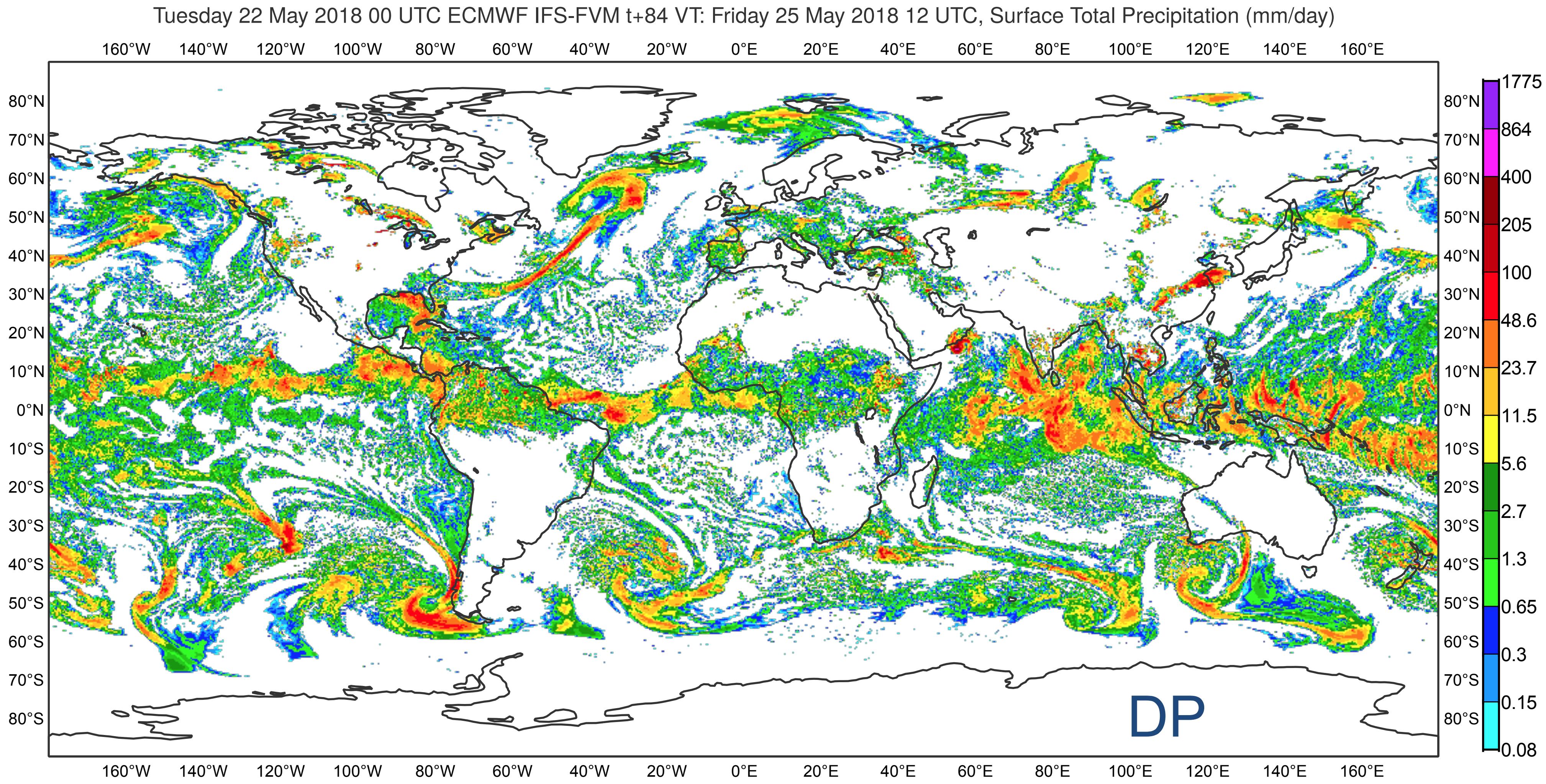

Geosci. Model Dev., 12, 651–676, 2019
https://doi.org/10.5194/gmd-12-651-2019

Geoscientific Model Development
Open Access

FVM 1.0: a nonhydrostatic finite-volume dynamical core for the IFS

Christian Kühnlein[1], Willem Deconinck[1], Rupert Klein[2], Sylvie Malardel[1,3], Zbigniew P. Piotrowski[4], Piotr K. Smolarkiewicz[1], Joanna Szmelter[5], and Nils P. Wedi[1]

[1]European Centre for Medium-Range Weather Forecasts, Reading, UK
[2]FB Mathematik und Informatik, Freie Universität Berlin, Berlin, Germany
[3]Laboratoire de l'Atmosphére et des Cyclones, Météo-France, La Reunion, France
[4]Institute of Meteorology and Water Management – National Research Institute, Warsaw, Poland
[5]Loughborough University, Leicestershire, LE11 3TU, UK

References

Smolarkiewicz P. K., W. Deconinck, M. Hamrud, C. Kühnlein, G. Modzinski, J. Szmelter, N. P. Wedi, A finite-volume module for simulating global all-scale atmospheric flows., J. Comput. Phys., 2016.

Kühnlein C., P. K. Smolarkiewicz, An unstructured-mesh finite-volume MPDATA for compressible atmospheric dynamics. J. Comput. Phys. 2017.

Deconinck W., P. Bauer, M. Diamantakis, M. Hamrud, C. Kühnlein, G. Mengaldo, P. Marciel, T. Quintino, B. Raoult, P. K. Smolarkiewicz, N. P. Wedi, Atlas: A library for numerical weather prediction and climate modelling, CPC, 2017.

Gillard M., Szmelter J., Cocetta F.: Preconditioning elliptic operators in high-performance all-scale atmospheric models on unstructured meshes, J. Comput. Phys., 2024.

Smolarkiewicz P. K., C. Kühnlein, W. Grabowski, A finite-volume module for cloud-resolving simulations of global atmospheric flows, J. Comput. Phys., 2017.

Smolarkiewicz P. K., C. Kühnlein, N. P. Wedi, Semi-implicit integrations of perturbation equations for all-scale atmospheric dynamics, J. Comput. Phys., 2019.

Kühnlein C., W. Deconinck, R. Klein, S. Malardel, Z.P. Piotrowski, P.K. Smolarkiewicz, J. Szmelter, N.P. Wedi, FVM 1.0: a nonhydrostatic finite-volume dynamical core for the IFS, Geosci. Model Dev., 12, 651-676, 2019.